

APPLICATIONS OF SLATTERY - LAGOUDAS' THEORY FOR THE STRESS
DEFORMATION BEHAVIOR

A Thesis

by

YONGZHE TIAN

Submitted to the Office of Graduate Studies of
Texas A&M University
in partial fulfillment of the requirements for the degree of

MASTER OF SCIENCE

August 2005

Major Subject: Aerospace Engineering

APPLICATIONS OF SLATTERY - LAGOUDAS' THEORY FOR THE STRESS
DEFORMATION BEHAVIOR

A Thesis

by

YONGZHE TIAN

Submitted to the Office of Graduate Studies of
Texas A&M University
in partial fulfillment of the requirements for the degree of

MASTER OF SCIENCE

Approved by:

Chair of Committee,	John C. Slattery
Committee Members,	Dimitris C. Lagoudas
	Vikram K. Kinra
	Ibrahim Karaman
Head of Department,	Helen L. Reed

August 2005

Major Subject: Aerospace Engineering

ABSTRACT

Applications of Slattery - Lagoudas' Theory for the Stress Deformation Behavior.

(August 2005)

Yongzhe Tian, B.En., Dalian University of Technology

Chair of Advisory Committee: Dr. John C. Slattery

The thermodynamics of three-dimensional, single-component elastic crystalline solids was developed by Slattery and Lagoudas (2005). Considering the infinitesimal deformations, the stress can be expressed as a function of the lattice vectors and density in the reference configuration and $\mu_{(I,mn)}$, which is defined as the derivative of specific Helmholtz free energy with respect to the $I_{(mn)}$. Using the Cauchy - Born rule to connect the interatomic potential energy and the specific Helmholtz free energy, it is possible to calculate the elastic properties of both nano-scale materials such as carbon nanotubes and macro-scale materials such as diamond and silicon. In this study, we used Tersoff (1988a) - Brenner (1990b) Potential, Tersoff (1988b) potential and Finnis and Sinclair (1984) potential for carbon, silicon, and vanadium systems respectively. Using the interatomic potentials to describe the specific Helmholtz free energy, the elastic properties of graphite, diamond, silicon and vanadium were calculated. This method was also extended to the calculation of Young's modulus of single-walled carbon nanotubes (SWCNTs), which are composed of a two dimensional array of carbon atoms. For SWCNT, we get good agreement with the available experimental data. For diamond and silicon, C_{11} and C_{12} were consistent with both the superelastic model and the experimental data. The difference of C_{44} between the calculation and experimental data was due to accuracy of the potential functions.

To Linda and Esther

ACKNOWLEDGMENTS

I would first like to show my gratitude to my advisor, Professor John C. Slattery, whose support and encouragement has been indispensable throughout the last two years. I would also like to thank Dr. Eun-Suok Oh, Kaibin Fu and Xiuhua Shi for discussion and useful comments in the process of this work. Also I would like to thank Professors Lagoudas, Kinra and Karaman for serving on my committee.

Especially, I want to thank my wife for her support and everything she has done for me.

TABLE OF CONTENTS

CHAPTER		Page
I	INTRODUCTION AND RESEARCH BACKGROUND	1
	A. Stress at equilibrium state	1
	B. The history of interatomic potentials	5
	C. Tersoff - Brenner potential	7
	D. Cauchy - Born rule	9
	E. Crystal elasticity	11
	1. Lattice configuration	11
	2. Lattice energy	12
II	ANOTHER FORM OF STRESS EXPRESSION	13
	A. Modified Gibbs and Gibbs-Duhem equations	13
	B. Mass balance	15
	C. Momentum balance	15
	D. Energy balance	15
	E. Entropy inequality	16
	F. Implication of equilibrium	17
III	ELASTIC PROPERTIES OF GRAPHITE	21
	A. Introduction	21
	B. Helmholtz free energy and interatomic potential energy	22
	C. Relationship between the stiffness tensor and the coefficients in the state function	23
	D. Structure and elastic properties of graphite	24
	1. Superelastic model	24
	2. New stress deformation behavior	28
	E. Single-walled carbon nanotubes	30
	F. Discussion	35
IV	ELASTIC PROPERTIES OF DIAMOND AND SILICON	38
	A. Structure of diamond and silicon	38
	B. Elastic properties of diamond	40
	C. Elastic properties of silicon	44
	1. Potential function for silicon bond	44

CHAPTER	Page
2. Elastic properties of silicon	45
V ELASTIC PROPERTIES OF VANADIUM	48
VI CONCLUSIONS	50
NOTATION	52
REFERENCES	55
VITA	63

LIST OF TABLES

TABLE		Page
I	Two sets of parameters of Tersoff - Brenner potential	8
II	Comparison of calculation and experimental data of C_{11} for graphite	27
III	C_{11} and Young's modulus considering the inner displacement and comparison with results from homogeneous deformation	28
IV	Reported elastic modulus of SWNT from experiment	34
V	Reported elastic modulus of SWNT from calculation	34
VI	Comparison of C_{11} and Young's modulus at different strain conditions - zigzag	37
VII	Inter displacement between two fcc sublattices under different axial strain conditions - diamond	42
VIII	Elastic properties of diamond(GPa)	44
IX	Parameters of Tersoff potential for silicon bonds	46
X	Inner displacement between two fcc sublattices under different axial strain conditions - silicon	46
XI	Elastic properties of silicon(GPa)	47
XII	Parameters of FS potential of vanadium	49
XIII	Elastic constants of vanadium by FS potential	49

LIST OF FIGURES

FIGURE	Page
1	Potential energy vs. bond length with coef1 - graphite 9
2	Potential energy vs. bond length with coef2 - graphite 10
3	Connection between Interatomic Potential Energy and Strain Energy through Cauchy - Born rule 21
4	Hexagonal bonding structure, π bond and σ bond. 25
5	A schematic diagram of structure of graphite. 26
6	Schematic of (a) a undeformed and (b) a deformed graphite layer by a homogenous deformation \mathbf{F} 29
7	Definition of roll-up vector as linear combination of base vector \bar{a}_1 and \bar{a}_2 31
8	The strain energy relative to the graphite vs. the radius of SW-CNT. Zero energy corresponds to the equilibrium graphite energy of -7.3756 eV/atom 32
9	The equilibrium position of zigzag nanotubes and comparison with graphite 32
10	The relationship between the radius of CNT and C_{11} , Young's modulus of zigzag CNT 35
11	The relationship between the radius of CNT and C_{11} , Young's modulus of armchair SWCNT 36
12	The relationship between the radius of CNT and Young's modulus 36
13	Interatomic potential energy vs. distance between atoms - diamond 39
14	Structure of diamond unit cell. The green and purple circles represent the atoms on the two different sublattices 39

FIGURE	Page
15 Young's modulus of diamond determined through stress strain curve	42
16 Potential energy vs. bond length - silicon	46

CHAPTER I

INTRODUCTION AND RESEARCH BACKGROUND

A. Stress at equilibrium state

Slattery and Lagoudas (2005) developed a new stress deformation behavior at equilibrium state. The natural configuration was chosen consistent with the following:

- The reference configuration is a stress free configuration.
- The reference configuration of each phase has the same mass as the current configuration of the phase.
- The boundary or a portion of boundary of the reference configuration moves as the phase transition progresses.

For each solid phase j , they assumed

$$\hat{A}^{(j)} = \hat{A}^{(j)}(T, \rho, \omega_1, \dots, \omega_{N-1}, \mathbf{E}_{(1)}^{(0)}, \mathbf{E}_{(2)}^{(0)}, \mathbf{E}_{(3)}^{(0)}, \dots, \mathbf{e}_{(1)}^{(j)}, \mathbf{e}_{(2)}^{(j)}, \mathbf{e}_{(3)}^{(j)} \dots) \quad (1.1)$$

Where \hat{A} is the Helmholtz free energy per unit mass, $E_{(i)}$ and $e_{(i)}$ are the lattice vector in the reference and current configuration respectively. A general form according to Truesdell and Noll (1965, p.29) is that the Helmholtz free energy is a function of all possible scalar products of the lattice vectors. Scalar products between the lattice vectors in reference and current configuration of different phases were eliminated since these would lead to non-symmetric stress tensor at equilibrium.

$$\hat{A}^{(j)} = \hat{A}^{(j)}(T, \rho, \omega_1, \dots, \omega_{N-1}, \mathbf{e}_{(1)}^{(j)} \cdot \mathbf{e}_{(1)}^{(j)}, \mathbf{e}_{(2)}^{(j)} \cdot \mathbf{e}_{(2)}^{(j)}, \dots, \mathbf{e}_{(3)}^{(j)} \cdot \mathbf{e}_{(3)}^{(j)}) \quad (1.2)$$

This thesis follows the style and format of *Mechanics of Materials*.

where \hat{A} is the Helmholtz free energy per unit mass, T the temperature, ρ the density, and

$$\mathbf{e}_{(i)} = \mathbf{F}\mathbf{E}_{(i)} \quad (1.3)$$

the current lattice vector, which is based on the Cauchy - Born rule (see more details in the next section).

It is more convenient to express the Helmholtz free energy as a function of six invariants:

$$I_{(mn)}^{(j)} \equiv \mathbf{e}_{(m)}^{(j)} \cdot \mathbf{e}_{(n)}^{(j)} - \mathbf{E}_{(m)}^{(j)} \cdot \mathbf{E}_{(n)}^{(j)} \quad (1.4)$$

Note that ρ and $I_{(11)}$, $I_{(22)}$ and $I_{(33)}$ are not independent.

In Slattery and Lagoudas (2005), they assumed that the Helmholtz free energy is a function of temperature (\mathbf{T}), density (ρ) and five other invariants. The Helmholtz free energy can be expressed as

$$\hat{A}^{(j)} = \hat{A}^{(j)}(T, \rho, \omega_{(1)}, \dots, \omega_{(N-1)}, I_{(11)}^{(j)}, I_{(22)}^{(j)}, I_{(12)}^{(j)}, I_{(13)}^{(j)}, I_{(23)}^{(j)}) \quad (1.5)$$

$$\check{A}^{(j)} = \check{A}^{(j)}(T, \hat{V}, \rho_{(1)}, \dots, \rho_{(N-1)}, I_{(11)}^{(j)}, I_{(22)}^{(j)}, I_{(12)}^{(j)}, I_{(13)}^{(j)}, I_{(23)}^{(j)}) \quad (1.6)$$

According to the differential entropy inequality (Slattery, 1999, p.438), they concluded

$$\hat{S} = - \left(\frac{\partial \hat{A}}{\partial T} \right)_{\rho, \omega_{(B)} (B \neq 1, \dots, N-1), I_{(mn)}} \quad (1.7)$$

Thermodynamic pressure (P) is defined as

$$P \equiv - \left(\frac{\partial \hat{A}}{\partial \hat{V}} \right)_{T, \omega_{(B)} (B \neq N), I_{(mn)}} \quad (1.8)$$

$\mu_{(I,mn)}$ is defined in the similar way as the chemical potential

$$\mu_{(I,mn)} \equiv - \left(\frac{\partial \hat{A}}{\partial I_{(mn)}} \right)_{T, \rho, \omega_{(B)} (B \neq N), I_{(rs)} (rs \neq mn)} \quad (1.9)$$

Based on the above definitions, they concluded that *Euler's equation* is

$$\hat{A} = -P\hat{V} + \sum_{B=1}^N \mu_{(B)} \omega_{(B)} \quad (1.10)$$

where μ_B is the chemical potential of specie B.

The modified Gibbs equation is given by

$$d\hat{A} = -Pd\hat{V} - \hat{S}dT + \sum_{B=1}^{N-1} (\mu_{(B)} - \mu_{(N)})d\omega_{(B)} + \sum_{m=1}^3 \sum_{n=1}^2 \mu_{(I,mn)}dI_{(mn)} \quad (1.11)$$

as well as the *modified Gibbs-Duhem equation*

$$-\hat{V}dP + \hat{S}dT + \sum_{B=1}^N \omega_{(B)}d\mu_{(B)} - \sum_{m=1}^3 \sum_{n=1}^2 \mu_{(I,mn)}dI_{(mn)} = 0 \quad (1.12)$$

Based on the above definitions and assumptions, they have (see Slattery and Lagoudas, 2005, eq.50)

$$\begin{aligned} & \int_R \left\{ \rho \left(\frac{1}{T} + \lambda_e \right) \frac{d_{(v)}\hat{U}}{dt} + \dots \right. \\ & \quad \left. + \frac{1}{T} \operatorname{tr} \left[\left(-T\lambda_e \mathbf{T} + \mathbf{PI} - \rho \sum_{\mathbf{m}=1}^3 \sum_{\mathbf{n}=1}^2 \mu_{(I,mn)} (\mathbf{e}_{(\mathbf{m})} \otimes \mathbf{e}_{(\mathbf{n})} + \mathbf{e}_{(\mathbf{n})} \otimes \mathbf{e}_{(\mathbf{m})}) \right) (\nabla \mathbf{v})^{\mathbf{T}} \right] \right\} d\mathbf{V} \\ & + \int_{\Sigma} \left\{ \left[(\dots)(\mathbf{v} - \mathbf{u}) \cdot \boldsymbol{\xi} \right] \right. \\ & \quad \left. - \sum_{k=1}^K \sum_{A=1}^N (\dots) \left(\frac{\partial \psi_{(k)}^{(\sigma)}}{\partial t} - \nabla_{(\sigma)} \psi_{(k)}^{(\sigma)} \cdot \mathbf{u} \right) \right\} d\mathbf{A} \geq 0 \end{aligned} \quad (1.13)$$

The transport theorem for a region containing a dividing surface was used in the derivation of equation (1.13). The general form was given in Slattery (1999), as shown in the following equation.

$$\frac{d}{dt} \int_{R(v)} \Psi dV = \int_{R(v)} \left(\frac{d_{(v)}\Psi}{dt} + \Psi \operatorname{div} \mathbf{v} \right) dV + \int_{\Sigma} [\Psi(\mathbf{v} - \mathbf{u}) \cdot \boldsymbol{\xi}] dA \quad (1.14)$$

where Ψ denotes a scalar, vector, or tensor. Σ indicates the dividing surface, and $\boldsymbol{\xi}$ is the normal of the dividing surface.

One condition that equation (1.13) must satisfy for equilibrium is

$$\mathbf{T} = -P\mathbf{I} + \rho \sum_{m=1}^3 \sum_{n=1}^2 \mu_{(I,mn)} (\mathbf{e}_{(m)} \otimes \mathbf{e}_{(n)} + \mathbf{e}_{(n)} \otimes \mathbf{e}_{(m)}) \quad (1.15)$$

where \mathbf{T} is the stress deformation behavior of elastic solids at equilibrium. In the appendix of Slattery and Lagoudas (2005), they introduced another form to use in the case of infinitesimal deformations. As a special case, \hat{A} can be expressed as a quadratic function of $I_{(11)}, \dots, I_{(33)}$ (Truesdell and Noll, 1965).

$$\hat{A} = c_{(0)} + \sum_{i=1}^3 \sum_{j=1}^2 c_{(ij)} I_{(ij)} + \frac{1}{2} \sum_{i=1}^3 \sum_{j=1}^2 \sum_{m=1}^3 \sum_{n=1}^2 a_{(ijmn)} I_{(ij)} I_{(mn)} + \dots \quad (1.16)$$

For this special case, the stress expression has the following form

$$\mathbf{T} = -P\mathbf{I} + 2\rho_0 \sum_{m=1}^3 \sum_{n=1}^2 \sum_{i=1}^3 \sum_{j=1}^2 a_{(ijmn)} (\mathbf{E}_{(i)} \cdot \mathbf{e}\mathbf{E}_{(j)}) (\mathbf{E}_{(m)} \otimes \mathbf{E}_{(n)} + \mathbf{E}_{(n)} \otimes \mathbf{E}_{(m)}) \quad (1.17)$$

where

$$\mathbf{e} = \frac{1}{2}(\nabla \mathbf{u} + (\nabla \mathbf{u})^T) \quad (1.18)$$

is the infinitesimal strain tensor, and \mathbf{u} is the displacement vector.

B. The history of interatomic potentials

Many problems in materials science and chemistry, such as surface reconstruction and mechanical properties, require a solution as a function of atomic position while including the information of total energy of the system of atoms. The quantum mechanical approach is quite accurate in this field. However, this method is not feasible for large systems due to intensive numerical calculations. Another approach is to construct an empirical interatomic potential, which is a function of atomic positions.

There are two kinds of interatomic potentials. One is the pair potential, such as the most commonly used Lennard-Jones potential (Hirschfelder et al., 1954, pg.22).

$$\phi^{(A,B)} = 4\epsilon^{(A,B)} \left[\left(\frac{\sigma^{(A,B)}}{r} \right)^{12} - \left(\frac{\sigma^{(A,B)}}{r} \right)^6 \right] \quad (1.19)$$

where $\phi^{(A,B)}$ is the potential of atoms A and B separated by a distance r . The r^{-6} term describes attractive force, while the r^{-12} term represents repulsive force.

Lennard-Jones potential is limited to rare gases, where atoms are connected only through van der Waals forces. The pair potential gives $C_{12} = C_{44}$, which is called the Cauchy relation.

The other kind is the many body potential for metals and semiconductors. Many body potentials had great success in predicting a wide range of properties accurately during the 80's (Catlow and Mackrodt, 1982; Daw and Baskes, 1984). The key point of this model is that the bonds become weaker with increasing coordination, which is also the consequence of the Pauli principle. The energy is proportional to the square root of the coordination, rather than to the coordination in the pair potential. Most many body potentials for metals have the general form as

$$V = \frac{1}{2} \sum_{i,j=1;j \neq i}^N \phi(r_{ij}) + \sum_{i=1}^N U(n_i) \quad (1.20)$$

where ϕ is the two body part, and U_n is a function of generalized coordination. However, these kinds of potentials are not applicable to the metals with strong covalent effects or semiconductors due to the lack of true angular forces.

For semiconductors, the most stable phase has the diamond structure, i.e., the coordination number is 4. The Stillinger - Weber potential (Stillinger and Weber, 1985) is one of the most widely used potentials for semiconductors. It has the form

$$V = \frac{1}{2} \sum_{ij} \phi(r_{ij}) + \sum_{ijk} g(r_{ij})g(r_{ik})(\cos \theta_{jik} + \frac{1}{3})^2 \quad (1.21)$$

where θ_{jik} is the angle between the $i - j$ bond and the $i - k$ bond, and $g(r_{ij})$ is a cutoff function. The last part obviously favors the configuration with $\theta_{jik} = \frac{1}{3}$, i.e., the angles close to those in diamond structure.

Abell (1985) derived a general form for potential energy, which is the sum of near neighbor pair interaction while considering the local atomic bonding environment. Tersoff (1988b) introduced an analytical expression based on Abell's form for silicon. The key point of this potential is that the strength of the bond is not only determined by two atoms, but also by the local environment included by bond order term. Brenner (1990b) gave two sets of parameters for carbon - carbon systems (Brenner, 1990a; Yin and Cohen, 1983a,b), which was used in this study for the calculation of elastic properties of graphite and diamond. The details of the Tersoff - Brenner potential will be given in chapter II.

We recommend two review papers for readers who might be interested in inter-atomic potentials. (Balamane et al. (1992) and Kane (1952))

C. Tersoff - Brenner potential

Tersoff (1988a) and Brenner (1990b) determined the interatomic potential for carbon as

$$\Phi(r_{ij}) = \Phi_R(r_{ij}) - B_{ij}\Phi_A(r_{ij}) \quad (1.22)$$

for atoms i and j , where r_{ij} is the distance between atoms i and j , Φ_R and Φ_A are the repulsive and attractive pair terms given by

$$\begin{aligned} \Phi_R(r_{ij}) &= \frac{D^e}{S-1} e^{-\sqrt{2S}\beta(r-R^e)} f_c(r_{ij}) \\ \Phi_A(r_{ij}) &= \frac{D^e S}{S-1} e^{-\sqrt{2/S}\beta(r-R^e)} f_c(r_{ij}) \end{aligned} \quad (1.23)$$

The parameters D^e , S, β and R^e are determined from the known physical properties. The function $f_c(r)$ is merely a smooth cutoff function to limit the range of the potential

$$f_c(r_{ij}) = \begin{cases} 1, & r_{ij} < R^{(1)} \\ 1/2(1 + \cos[\frac{\pi(r-R^{(1)})}{R^{(2)}-R^{(1)}}]), & R^{(1)} < r_{ij} < R^{(2)} \\ 0, & r_{ij} > R^{(2)} \end{cases} \quad (1.24)$$

which restricts the potential to the first-neighbor shell.

The parameter B_{ij} in (1.22) represents a multi-body coupling between the bond from atom i to atom j and the local environment of atom i , and is given by

$$B_{ij} = \left[1 + \sum_{k(\neq i,j)} G(\theta_{ijk}) f_c(r_{ik}) \right]^{-\delta} \quad (1.25)$$

where r_{ik} is the distance between atoms i and k , θ_{ijk} is the angle between $i-j$ bond and $j-k$ bond, and the function G is given by

Table I. Two sets of parameters of Tersoff - Brenner potential

	<i>Coeff1</i> ^(a)	<i>Coeff2</i> ^(b)
D^e	6.325 eV	6.000 eV
S	1.29	1.22
β	15 nm ⁻¹	21 nm ⁻¹
R^e	0.1315 nm	0.1390 nm
δ	0.80469	0.50000
a_0	0.011304	0.00021
c_0	19	330
d_0	2.8	3.5

(a) fit to Brenner (1990a)

(b) fit to Yin and Cohen (1983b,a)

$$G(\theta_{ijk}) = a_0 \left[1 + \frac{c_0^2}{d_0^2} - \frac{c_0^2}{d_0^2 + (1 + \cos \theta)^2} \right] \quad (1.26)$$

For atoms i and j having different local environment, Brenner (1990b) suggested replacing coefficient B_{ij} in (1.26) by

$$\bar{B}_{ij} = \frac{B_{ij} + B_{ji}}{2} \quad (1.27)$$

The parameters D^e , S , β and R^e in (1.23) and (1.24), δ in (1.26), and a_0 , c_0 and d_0 in (1.27) have been determined by Brenner (1990b). In fact, Brenner (1990b) gave two sets of parameters for carbon as shown in Table I.

The equilibrium bond length, donated by l_0 is determined by minimizing the interatomic potential

$$\frac{\partial \Phi}{\partial r_{ij}} = 0 \quad (1.28)$$

This gives the equilibrium bond length as $l_0 = 0.142nm$ and $l_0 = 0.145nm$ for the

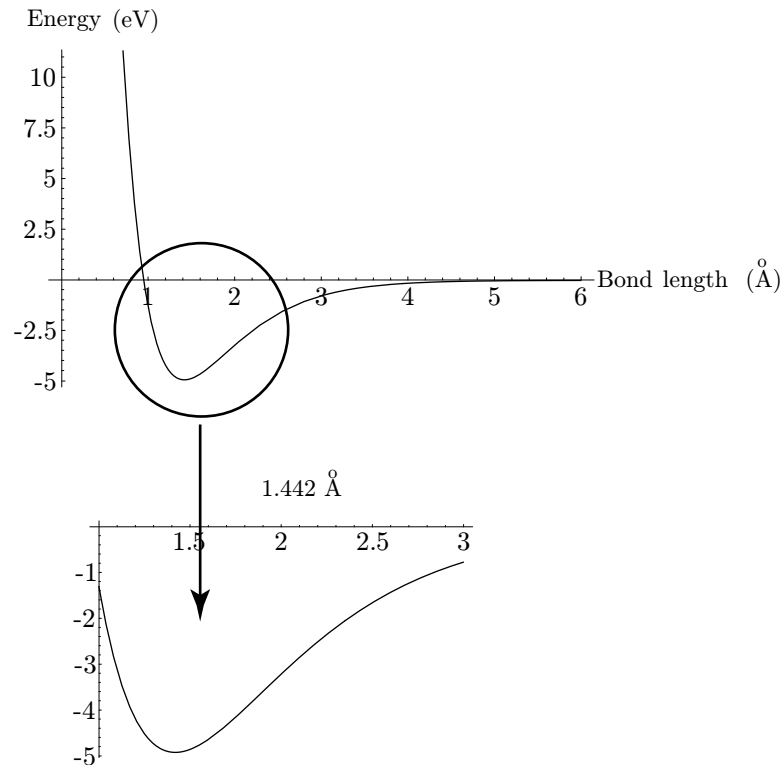


Fig. 1. Potential energy vs. bond length with coef1 - graphite

two sets of parameters, as shown in fig. 1 and fig. 2, respectively. Both results are consistent with the well known bond length of graphite ($0.144nm$). It should be noted that all the results given in this study were calculated by the second set of parameters.

D. Cauchy - Born rule

The Cauchy - Born rule is an assumption made in the analysis of Slattery and Lagoudas (2005), as given in (1.3). The objective of the Cauchy - Born rule is to set up a connection between the elastic theory and molecular theory (molecular description of crystalline configuration). This assumption goes back to Cauchy (1828), who assumed that the atomic motion agrees with the gross deformation. Born (1915)

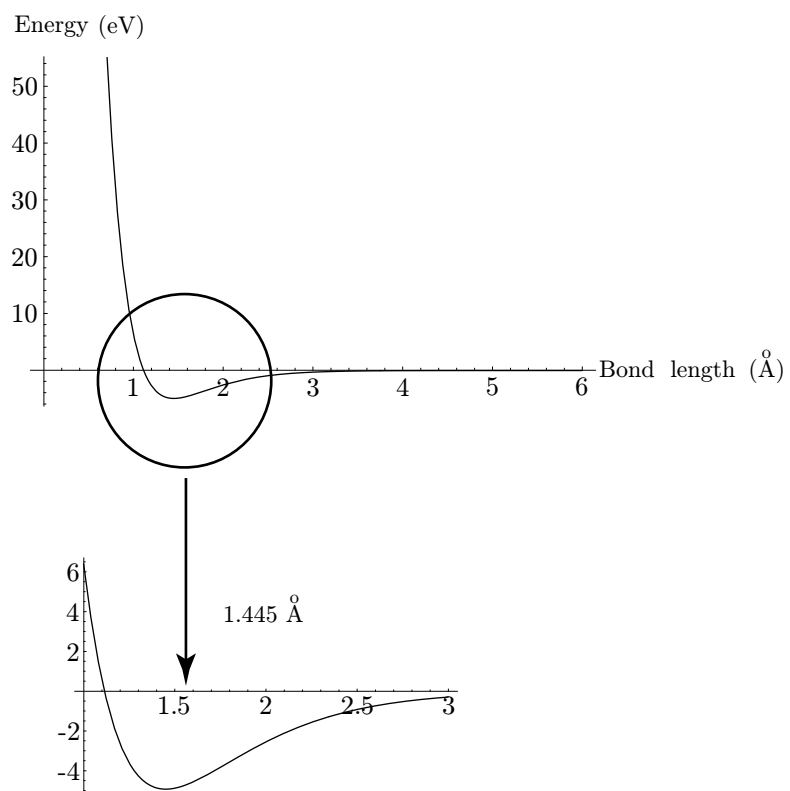


Fig. 2. Potential energy vs. bond length with coef2 - graphite

concluded that this is not always true and made another assumption that only the skeletal structure of crystalline lattices is embedded in the macroscopic deformation, which is referred as the Cauchy-Born rule (see also Born and Huang (1954)). Skeletal lattices are analogs to the external lattices in Oh et al. (2005). Ericksen (1984) pointed out that the Cauchy Born rule is equivalent to the assumption of homogeneous deformation. Zanzotto (1996) concluded that the Born rule always holds for crystals whose structure can be described by a simple Bravais lattice and shape memory alloys.

The Born rule states that the skeletal lattice vectors deform as material vectors, which indicates that they are embedded in the macroscopic deformation. The deformed skeletal lattice vectors $e_{(i)}, i = 1...3$ are defined by (1.3), which allows one to go back and forth between the current lattices and macroscopic deformation.

E. Crystal elasticity

1. Lattice configuration

Most solids have the configuration of a periodic array of atoms, which are called lattice vectors. The simplest repeating unit is called a *unit cell*. In 1850, Auguste Bravais showed that crystals can be divided into 14 unit cells. 3 - D *Bravais lattices* consisted of all points with position vector \mathbf{R} defined as

$$\mathbf{R} \equiv n_1 \mathbf{a}_1 + n_2 \mathbf{a}_2 + n_3 \mathbf{a}_3 \quad (1.29)$$

where $\mathbf{a}_i (i = 1, 2, 3)$ are primitive lattice vectors. A primitive unit cell is the smallest parallelepiped with an atom at each corner, i.e., only one atom per primitive cell.

Any lattice structures more complicated than 14 Bravais lattices can be considered as a number of interpenetrating simple Bravais lattices. The position vectors

given by

$$\mathbf{x} = \sum_{\mathbf{a}} M^{\mathbf{a}} \mathbf{e}_{(\mathbf{a})} + \mathbf{p}_{\mathbf{k}} \quad (1.30)$$

where $M^{\mathbf{a}}$ are integers ($\mathbf{a}=1,2,3$), $\mathbf{e}_{(\mathbf{a})}$ are skeletal lattice vectors, and $\mathbf{p}_{\mathbf{k}}$ are *shift vectors*. Shift vectors are also interpreted as structure *motif* (Zanzotto, 1996).

2. Lattice energy

The Helmholtz free energy density per unit mass \hat{A} in the isothermal condition is a function of lattice vectors $\mathbf{e}_{(\mathbf{a})}$ and $\mathbf{p}_{\mathbf{k}}$

$$\hat{A} = \hat{A}(\mathbf{e}_{(\mathbf{a})}, \mathbf{p}_{\mathbf{k}}) \quad (1.31)$$

$\mathbf{p}_{\mathbf{k}}$ can be eliminated from the energy function by minimization of \hat{A} (Parry, 1981; Zanzotto, 1996).

According to the Cauchy - Born rule, the energy density becomes

$$\hat{A} = \hat{A}(\mathbf{e}_{(\mathbf{a})}) \quad (1.32)$$

This approach was also used by Ericksen (1980) and James (1987). It is also consistent with Barron et al. (1971) and Keating (1968).

This assumption is also used in this study to calculate the elastic properties of graphite, SWCNT, diamond and silicon.

CHAPTER II

ANOTHER FORM OF STRESS EXPRESSION

A. Modified Gibbs and Gibbs-Duhem equations

The thermodynamic pressure was introduced (Slattery and Lagoudas, 2005) in order to be consistent with the standard development of the Gibbs Phase rule (Denbigh, 1963). However, it is more convenient to eliminate pressure terms in the stress expression for applications in this study. The independent variables of a specific Helmholtz free energy are invariants, temperature and mass fractions. Equations (1.5) and (1.6) become

$$\hat{A}^{(j)} = \hat{A}^{(j)}(T, \omega_{(1)}, \dots, \omega_{(N-1)}, I_{(11)}^{(j)}, I_{(22)}^{(j)}, I_{(12)}^{(j)}, I_{(13)}^{(j)}, I_{(23)}^{(j)}, I_{(33)}^{(j)}) \quad (2.1)$$

$$\check{A}^{(j)} = \check{A}^{(j)}(T, \rho_{(1)}, \dots, \rho_{(N-1)}, I_{(11)}^{(j)}, I_{(22)}^{(j)}, I_{(12)}^{(j)}, I_{(13)}^{(j)}, I_{(23)}^{(j)}, I_{(33)}^{(j)}) \quad (2.2)$$

With the above assumptions, the differentials of (2.1) and (2.2) can be expressed as

$$\begin{aligned} d\hat{A} = & -\hat{S}dT + \sum_{B=1}^{N-1} \left(\frac{\partial \hat{A}}{\partial \omega_{(B)}} \right)_{T, \omega_{(C)} (C \neq B, N), I_{(mn)}} d\omega_{(B)} \\ & + \sum_{m=1}^3 \sum_{n \geq m}^3 \mu_{(I, mn)} dI_{(mn)} \end{aligned} \quad (2.3)$$

$$d\check{A} = -\frac{\check{S}}{\check{V}}dT + \sum_{B=1}^{N-1} \mu_{(B)} d\rho_{(B)} + \frac{1}{\check{V}} \sum_{m=1}^3 \sum_{n \geq m}^3 \mu_{(I, mn)} dI_{(mn)} \quad (2.4)$$

Equation (2.4) may be rearranged to read

$$\begin{aligned}
d\left(\frac{\hat{A}}{\hat{V}}\right) &= -\frac{\hat{S}}{\hat{V}}dT + \sum_{B=1}^{N-1} \mu_{(B)}d\left(\frac{\omega_{(B)}}{\hat{V}}\right) \\
&\quad + \frac{1}{\hat{V}} \sum_{m=1}^3 \sum_{n \geq m}^3 \mu_{(I,mn)}dI_{(mn)}
\end{aligned} \tag{2.5}$$

$$\begin{aligned}
d\hat{A} &= \left(\frac{\hat{A}}{\hat{V}} - \sum_{B=1}^{N-1} \mu_{(B)}\rho_{(B)}\right)d\hat{V} - \hat{S}dT \\
&\quad + \sum_{B=1}^{N-1} \mu_{(B)}d\omega_{(B)} + \sum_{m=1}^3 \sum_{n \geq m}^3 \mu_{(I,mn)}dI_{(mn)}
\end{aligned} \tag{2.6}$$

Comparison of the coefficients in (2.3) and (2.6) gives *Euler's equation*

$$\hat{A} = \sum_{B=1}^{N-1} \mu_{(B)}\omega_{(B)} \tag{2.7}$$

Equation (2.7) gives the *modified Gibbs equation*

$$d\hat{A} = -\hat{S}dT + \sum_{B=1}^{N-1} \mu_{(B)}d\omega_{(B)} + \sum_{m=1}^3 \sum_{n \geq m}^3 \mu_{(I,mn)}dI_{(mn)} \tag{2.8}$$

The *modified Gibbs - Duhem equation* can be obtained by subtracting (2.8) from the differential of (2.7):

$$\hat{S}dT + \sum_{B=1}^{N-1} \omega_{(B)}d\mu_{(B)} - \sum_{m=1}^3 \sum_{n \geq m}^3 \mu_{(I,mn)}dI_{(mn)} = 0 \tag{2.9}$$

In this study, we focused on the static crystalline solid with single component. We assumed that the Helmholtz free energy is only a function of temperature and six invariants.

B. Mass balance

The mass balance requires that the time rate change of the mass is zero without chemical reactions (Slattery, 1999, pg.679)

$$\frac{d}{dt} \int_R \rho \omega_{(A)} dV = 0 \quad (2.10)$$

where R means the region occupied by the body. Using the transport theorem (1.14), $Z_{(A)}$ was defined as

$$Z_{(A)} \equiv \int_R \rho \frac{d_{(v)} \omega_{(A)}}{dt} dV + \int_{\Sigma} [\rho \omega_{(A)} (\mathbf{v} - \mathbf{u}) \cdot \boldsymbol{\xi}] dA = 0 \quad (2.11)$$

where Σ means the internal phase interface.

C. Momentum balance

The momentum balance requires (Slattery, 1999, pg. 709)

$$\frac{d}{dt} \int_R \rho \mathbf{v} dV = \int_S \mathbf{T} \mathbf{n} dA + \int_R \rho \mathbf{f} dV \quad (2.12)$$

Apply the transport theorem and define \mathbf{Z}_m as

$$\begin{aligned} \mathbf{Z}_m &\equiv \int_R \left[\rho \frac{d_{(v)} \mathbf{v}}{dt} - \operatorname{div} \mathbf{T} - \rho \mathbf{f} \right] dV + \int_{\Sigma} [\rho \mathbf{v} (\mathbf{v} - \mathbf{u}) \cdot \boldsymbol{\xi} - \mathbf{T} \boldsymbol{\xi}] dA \\ &= 0 \end{aligned} \quad (2.13)$$

D. Energy balance

For the static isolated body, the energy balance (Slattery, 1990, pg. 716) requires that

$$\begin{aligned}
\frac{d}{dt} \int_R \rho \left(\hat{U} + \frac{1}{2} v^2 \right) dV &= \int_S \mathbf{v} \cdot \mathbf{T} \mathbf{n} dA \\
&= \int_R [\mathbf{v} \cdot \operatorname{div} \mathbf{T} + \operatorname{tr}(\mathbf{T} \nabla \mathbf{v})] dV + \int_\Sigma [\mathbf{v} \cdot \mathbf{T} \boldsymbol{\xi}] dA \quad (2.14)
\end{aligned}$$

The left hand side of the above equation can be expressed as

$$\frac{d}{dt} \int_R \rho \left(\hat{U} + \frac{1}{2} v^2 \right) dV = \int_R \left[\rho \frac{d_{(v)}}{dt} \left(\hat{U} + \frac{1}{2} v^2 \right) \right] dV + \int_\Sigma \rho \left(\hat{U} + \frac{1}{2} v^2 \right) (\mathbf{v} - \mathbf{u}) \cdot \boldsymbol{\xi} \, dA \quad (2.15)$$

Define Z_e as

$$\begin{aligned}
Z_e &\equiv \int_R \left\{ \rho \frac{d_{(v)} \hat{E}}{dt} - \mathbf{v} \cdot (\operatorname{div} \mathbf{T} + \rho) - \operatorname{tr}(\mathbf{T} \nabla \mathbf{v}) \right\} dV \\
&\quad + \int_\Sigma \left[\rho \hat{E} (\mathbf{v} - \mathbf{u}) \cdot \boldsymbol{\xi} - \mathbf{v} \cdot \mathbf{T} \boldsymbol{\xi} \right] dA \\
&= 0 \quad (2.16)
\end{aligned}$$

where \hat{E} is total energy per unit mass

$$\hat{E} \equiv \hat{U} + \frac{1}{2} v^2 \quad (2.17)$$

E. Entropy inequality

For the isolated body, the entropy inequality (Truesdell and Toupin, 1960, pg.644), i.e., the second law of thermodynamics, requires that the time rate change of entropy must be greater than or equal to zero:

$$\frac{d}{dt} \int_R \rho \hat{S} dV \geq 0 \quad (2.18)$$

Applying the transport theorem again, (2.18) may be written as

$$\int_R \rho \frac{d_{(v)} \hat{S}}{dt} dV + \int_{\Sigma} [\rho \hat{S}(\mathbf{v} - \mathbf{u}) \cdot \boldsymbol{\xi}] dA \geq 0 \quad (2.19)$$

F. Implication of equilibrium

If equilibrium is to be achieved, the left hand side of (2.18) must be minimized with the constraints imposed by conservation of mass (2.11), the momentum balance (2.13), and the energy balance (2.16).

$$\int_R \frac{d_{(v)} \hat{S}}{dt} dV + \int_{\Sigma} [\rho \hat{S}(\mathbf{v} - \mathbf{u}) \cdot \boldsymbol{\xi}] dA + \lambda_A Z_A + \boldsymbol{\lambda}_m \cdot \mathbf{Z}_m + \lambda_e Z_e \geq 0 \quad (2.20)$$

where λ_A , $\boldsymbol{\lambda}_m$ and λ_e are lagrangian multipliers.

From (2.8) and the definition of \hat{A} (Slattery, 1999, pg. 446)

$$\frac{d_{(v)} \hat{S}}{dt} = \frac{1}{T} \frac{d_{(v)} \hat{U}}{dt} - \frac{1}{T} \sum_{A=1}^{N-1} \mu^{(A)} \frac{d_{(v)} \omega^{(A)}}{dt} - \frac{1}{T} \sum_{m=1}^3 \sum_{n \geq m}^3 \mu_{(I, mn)} \frac{d_{(v)} I_{(mn)}}{dt} \quad (2.21)$$

The last term in equation (2.21) is derived from definition of $I_{(mn)}$

$$\begin{aligned} \frac{d_{(v)} I_{(mn)}}{dt} &= \nabla \mathbf{v} \mathbf{e}_{(m)} \cdot \mathbf{e}_{(n)} + \mathbf{e}_{(m)} \cdot \nabla \mathbf{v} \mathbf{e}_{(n)} \\ &= \text{tr} [(\mathbf{e}_{(m)} \otimes \mathbf{e}_{(n)} + \mathbf{e}_{(n)} \otimes \mathbf{e}_{(m)}) \nabla \mathbf{v}] \end{aligned} \quad (2.22)$$

After rearranging (2.20) by means of (2.22), (2.21) and (2.17), we have

$$\begin{aligned}
& \int_R \left\{ \rho \left(\frac{1}{T} + \lambda_e \right) \frac{d_{(v)} \hat{U}}{dt} + \dots \right. \\
& \quad \left. + \frac{1}{T} \operatorname{tr} \left[\left(-T \lambda_e \mathbf{T} - \rho \sum_{\mathbf{m}=1}^3 \sum_{\mathbf{n} \geq \mathbf{m}}^3 \mu_{(\mathbf{I}, \mathbf{mn})} (\mathbf{e}_{(\mathbf{m})} \otimes \mathbf{e}_{(\mathbf{n})} + \mathbf{e}_{(\mathbf{n})} \otimes \mathbf{e}_{(\mathbf{m})}) \right) (\nabla \mathbf{v})^{\mathbf{T}} \right] \right\} d\mathbf{V} \\
& + \int_{\Sigma} [(\dots)(\mathbf{v} - \mathbf{u}) \cdot \boldsymbol{\xi}] dA \geq 0
\end{aligned} \tag{2.23}$$

At equilibrium, we have a different stress expression

$$\mathbf{T} = \rho \sum_{\mathbf{m}=1}^3 \sum_{\mathbf{n} \geq \mathbf{m}}^3 \mu_{(\mathbf{I}, \mathbf{mn})} (\mathbf{e}_{(\mathbf{m})} \otimes \mathbf{e}_{(\mathbf{n})} + \mathbf{e}_{(\mathbf{n})} \otimes \mathbf{e}_{(\mathbf{m})}) \tag{2.24}$$

In the limit of infinitesimal deformations, we have

$$\mathbf{T} = 2\rho_0 \sum_{m=1}^3 \sum_{n \geq m}^3 \sum_{i=1}^3 \sum_{j \geq i}^3 a_{(ijmn)} (\mathbf{E}_{(i)} \cdot \mathbf{e} \mathbf{E}_{(j)}) (\mathbf{E}_{(m)} \otimes \mathbf{E}_{(n)} + \mathbf{E}_{(n)} \otimes \mathbf{E}_{(m)}) \tag{2.25}$$

The difference between the two is the elimination of the pressure term and the range of the summation term.

Now the stress expression is only a function of density and lattice vectors in the reference configuration. The unknowns are coefficients in the quadratic state function. In this study, the coefficients were determined by the second derivative of interatomic potentials with respect to the invariants.

We also recognized that for the system without a dividing surface, the integration Σ will disappear. The stress expression comes from the balance of energy and entropy inequality.

The same result can be derived only through the entropy inequality and differential energy balance for an isothermal system.

The differential entropy inequality is given by

$$\rho T \frac{d_{(v)} \hat{S}}{dt} \geq -T \operatorname{div} \left(\frac{\mathbf{e}}{T} \right) + \rho Q \quad (2.26)$$

where \mathbf{e} is the thermal energy flux vector.

Now subtract (2.26) from the differential energy balance (Slattery, 1999, p.255)

$$\rho \frac{d_{(v)} \hat{U}}{dt} = \operatorname{div}(\mathbf{q}) + \operatorname{tr}(\mathbf{T} \cdot \nabla \mathbf{v}) + \rho Q \quad (2.27)$$

where \mathbf{q} is energy flux vector.

We have

$$\rho \frac{d_{(v)} \hat{U}}{dt} - \rho T \frac{d_{(v)} \hat{S}}{dt} - \operatorname{tr}(\mathbf{T} \cdot \nabla \mathbf{v}) + \operatorname{div}(\mathbf{q} - \mathbf{e}) + \frac{1}{T} \mathbf{e} \cdot \nabla T \leq 0 \quad (2.28)$$

It more convenient to write (2.28) in terms of the Helmholtz free energy per unit mass

$$\rho \frac{d_{(v)} \hat{A}}{dt} + \rho \hat{S} \frac{d_{(v)} \hat{T}}{dt} - \operatorname{tr}(\mathbf{T} \cdot \nabla \mathbf{v}) + \operatorname{div}(\mathbf{q} - \mathbf{e}) + \frac{1}{T} \mathbf{e} \cdot \nabla T \leq 0 \quad (2.29)$$

Here we only consider the single component system for simplicity.

$$\hat{A} = \hat{A}(T, I_{(11)}, I_{(22)}, I_{(33)}, I_{(23)}, I_{(13)}, I_{(12)}) \quad (2.30)$$

The differential of (2.30) may consequently be expressed as

$$d\hat{A} = -\hat{S}dT + \sum_{m=1}^3 \sum_{n \geq m}^3 \mu_{(I, mn)} dI_{(mn)} \quad (2.31)$$

$$\frac{d_{(v)} \hat{A}}{dt} = -\hat{S} \frac{d_{(v)} \hat{T}}{dt} + \sum_{m=1}^3 \sum_{n \geq m}^3 \mu_{(I, mn)} \frac{d_{(v)} I_{(mn)}}{dt} \quad (2.32)$$

Now rearrange (2.29) for an isothermal system

$$\rho \sum_{m=1}^3 \sum_{n \geq m}^3 \frac{d_{(v)} I_{(mn)}}{dt} - tr(\mathbf{T} \cdot \nabla \mathbf{v}) \leq 0 \quad (2.33)$$

where $d_{(v)} I_{(mn)}/dt$ is given by

$$\frac{d_{(v)} I_{(mn)}}{dt} = tr[(\mathbf{e}_{(m)} \otimes \mathbf{e}_{(n)} + \mathbf{e}_{(n)} \otimes \mathbf{e}_{(m)}) \nabla \mathbf{v}] \quad (2.34)$$

Entropy inequality becomes equality at the equilibrium state. It is clear from the above two equations that

$$\mathbf{T} = \rho \sum_{m=1}^3 \sum_{n \geq m}^3 (\mathbf{e}_{(m)} \otimes \mathbf{e}_{(n)} + \mathbf{e}_{(n)} \otimes \mathbf{e}_{(m)}) \quad (2.35)$$

(2.35) is the same as equation (1.15) for infinitesimal deformations. It's just the simplified derivation for the special case, rather than the substitution of the result from Slattery and Lagoudas (2005).

The objective in what follows is to use this stress expression to calculate the elastic properties of graphite, single-walled carbon nanotubes, diamond, silicon and vanadium by using the Tersoff - Brenner potential (Tersoff, 1988a; Brenner, 1990b), Tersoff potential (Tersoff, 1988b) and Finnis - Sinclair potential (Finnis and Sinclair, 1984) respectively.

In Chapter III, I calculated the elastic properties of graphite and compared the results with the superelastic model and the experimental data. In this study, *super-elastic* was used in order to be consistent with literature, such as Zhang et al. (2002).

In Chapter IV and Chapter V, the elastic properties of diamond, silicon and vanadium were calculated. The results are consistent with the superelastic model. For diamond and silicon, the difference of C_{44} between the calculation and the experimental data was due to the accuracy of the potential function. With several applications of this new stress expression we could visualize more prospects for further application.

CHAPTER III

ELASTIC PROPERTIES OF GRAPHITE

A. Introduction

It is commonly accepted that continuum mechanics is not applicable to the atomic scale materials because the scales fall far beyond the frames of continuum mechanics. However, the confidence comes from the incorporation of interatomic potentials.

The first attempt to derive elastic constants from the potential energy of a crystal system were made by Born and Huang (1954). Based on Brugger's thermodynamic definition of elastic constants (Brugger, 1964, eq.2), Martin (1975a,b,c) derived elastic constants for a crystal system in which the energy density is a sum of bonds. Zhang et al. (2002) and Belytschko et al. (2002) incorporated interatomic potentials into a continuum theory. In the calculation, the interatomic potential and stored strain energy density on a continuum level is evaluated by the bond energy on the atomic level through the Tersoff - Brenner potential for all bonds in the unit cell while using the Cauchy - Born rule (Tadmor et al., 1996; James and Hane, 2000), as shown in fig. 3. As a brief summary, if the energy density, W , of the material is known, the relation

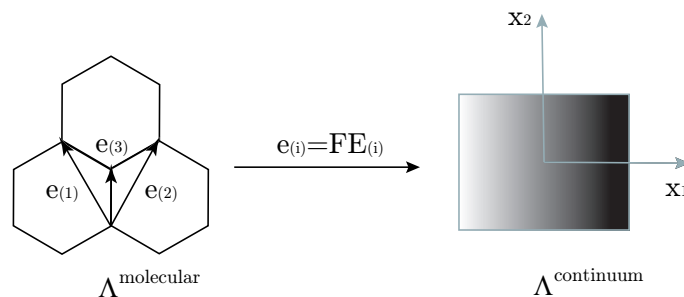


Fig. 3. Connection between Interatomic Potential Energy and Strain Energy through Cauchy - Born rule

between the stress (\mathbf{T}) and the deformation gradient (\mathbf{F}) is given by Belytschko et al. (2000)

$$P_{ij} = \frac{\partial W}{\partial F_{ij}} \quad (3.1)$$

In (3.1), $F_{ij} = \partial x_i / \partial X_j$, in which x and X are the spatial and material coordinates, respectively. An equivalent form is to express this in terms of the second Piola-Kirchhoff stress S and the Lagrangian strain \mathbf{E}

$$S_{ij} = \frac{\partial W}{\partial E_{ij}} \quad (3.2)$$

The corresponding stiffness tensor is

$$C_{ijkl} = \frac{\partial^2 W}{\partial E_{ij} \partial E_{kl}} \quad (3.3)$$

To apply superelasticity to the crystal system, the Cauchy - Born rule must be imposed. This rule assumes that the local crystal structure deforms homogenously. Using these assumptions, the stiffness tensor defined above can be used in atomic-scale systems.

B. Helmholtz free energy and interatomic potential energy

The specific Helmholtz free energy is defined as (3.4)

$$\hat{A} \equiv \hat{U} - T\hat{S} \quad (3.4)$$

$$d\hat{A} = d\hat{U} - Td\hat{S} - \hat{S}dT \quad (3.5)$$

Considering an isothermal equilibrium state, in which the entropy can be ex-

pressed only as the function of temperature (Hill, 1962), the last two terms in equation (3.5) are zero.

The internal energy is composed of the kinetic energy and the potential energy. For an isothermal system, the kinetic energy is a constant.

$$d\hat{U} = d\Phi \quad (3.6)$$

where Φ is the interatomic potential energy.

We can use (3.6) to rewrite (3.5)

$$d\hat{A} = d\Phi \quad (3.7)$$

Equation (3.7) means that the change of Helmholtz free energy due to the macroscopic deformation is the same as the change of interatomic potential energy.

C. Relationship between the stiffness tensor and the coefficients in the state function

For linear elastic solids, Hooke's law gives

$$\mathbf{T} = \mathbf{C}\epsilon \quad (3.8)$$

where \mathbf{C} is elastic stiffness tensor. Using Einstein index notation, it can be expressed as

$$T_{pq} = C_{pqrs}\epsilon_{rs} \quad (3.9)$$

Now express new stress using index notation:

$$T_{pq} = 2\rho_0 \sum_{m=1}^3 \sum_{n \geq m}^3 \sum_{i=1}^3 \sum_{j \geq i}^3 a_{(ijkl)} (E_{(i)r} E_{(j)s}) (E_{(k)p} E_{(l)q} + E_{(l)p} E_{(k)q}) \epsilon_{rs} \quad (3.10)$$

Comparing the above two equations, the relationship is given in the following:

$$C_{pqrs} = 2\rho_0 \sum_{m=1}^3 \sum_{n \geq m}^3 \sum_{i=1}^3 \sum_{j \geq i}^3 a_{(ijkl)} (E_{(i)r} E_{(j)s}) (E_{(k)p} E_{(l)q} + E_{(l)p} E_{(k)q}) \quad (3.11)$$

D. Structure and elastic properties of graphite

In graphite, sp^2 hybridization occurs, which means one s-orbital and two p-orbitals combine to form three sp^2 orbitals at 120° from each other within a plane. This kind of bond is also called a σ bond. A σ bond is a strong covalent bond which results in the high stiffness and high strength in the graphite plane. The remaining p-orbital is perpendicular to the σ bond plane which is called the π bond. This interlayer π bond is much weaker than the σ bond. The bond structure is shown in fig. 4.

1. Superelastic model

Using the Cauchy - Born rule to connect the interatomic potential energy and strain energy requires the centrosymmetry structure (Zhang et al., 2002), i.e. , each atom can be viewed as the center of structure, or each of them has the same bonding environment (Oh et al., 2005). It is obvious that the graphite structure, which is composed of hexagonal lattices, is not centrosymmetric. As shown in fig. 5, A and B indicate two sublattices. Both of them have the triangular structure or can be viewed as a hexagon with one atom in the center. In this case, Cousins (1978) and Martin (1975a,b,c) pointed out that the inner displacement between the two sublattices should be considered. The continuum model that accounts for this effect

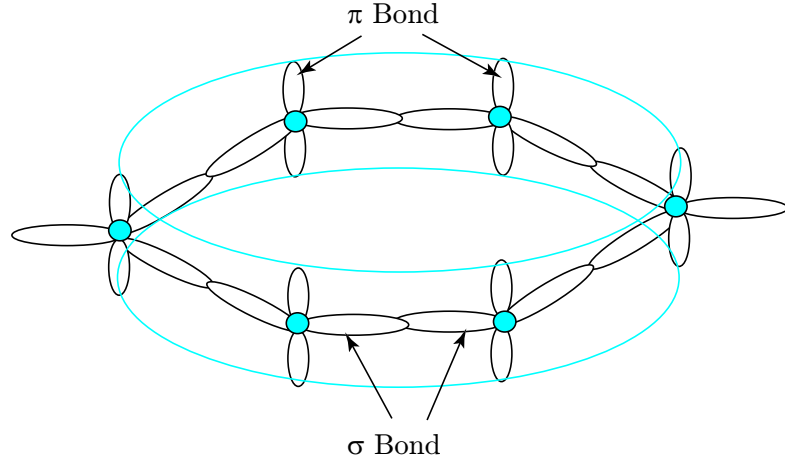


Fig. 4. Hexagonal bonding structure, π bond and σ bond.

was introduced by Zhang et al. (2002).

As a summary, an arbitrary vector \mathbf{R}_{ij}^0 from point i in sublattice A to j under the uniform deformation \mathbf{F} becomes $\mathbf{F} \cdot \mathbf{R}_{ij}^0$. Besides the homogeneous deformation, sublattice B may have a relative displacement with respect to sublattice A. In his paper, the distance between i and j becomes

$$\begin{aligned} r_{ij} &= \sqrt{(\mathbf{R}_{ij}^0 + \mathbf{x}) \cdot \mathbf{F}^T \cdot \mathbf{F} \cdot (\mathbf{R}_{ij}^0 + \mathbf{x})} \\ &= \sqrt{(\mathbf{R}_{ij}^0 + \mathbf{x}) \cdot (\mathbf{I} + 2\mathbf{E}) \cdot (\mathbf{R}_{ij}^0 + \mathbf{x})} \end{aligned} \quad (3.12)$$

where \mathbf{E} is the Lagrangian strain tensor.

The modified Cauchy - Born rule is expressed as:

$$\mathbf{C} = \frac{\partial^2 \Phi}{\partial \mathbf{E}^2} + \frac{\partial^2 \Phi}{\partial \mathbf{E} \partial \mathbf{x}} \frac{\partial \mathbf{x}}{\partial \mathbf{E}} \quad (3.13)$$

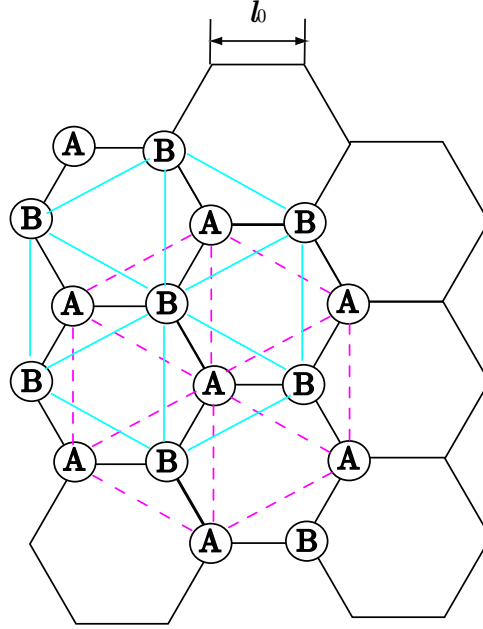


Fig. 5. A schematic diagram of structure of graphite.

where \mathbf{x} is the inner displacement between the sublattices. It can be determined by the minimization of the interatomic potential energy with respect to \mathbf{x} , i.e.,

$$\frac{\partial \Phi}{\partial \mathbf{x}} = 0 \quad (3.14)$$

the term $\partial \mathbf{x} / \partial \mathbf{E}$ is given

$$\frac{\partial \mathbf{x}}{\partial \mathbf{E}} = - \left(\frac{\partial^2 \Phi}{\partial \mathbf{x}^2} \right)^{-1} \frac{\partial^2 \Phi}{\partial \mathbf{x} \partial \mathbf{E}} \quad (3.15)$$

Zhang et al. (2002) concluded that the elastic modulus is

$$\mathbf{C} = \left[\frac{\partial^2 \Phi}{\partial \mathbf{E}^2} - \frac{\partial^2 \Phi}{\partial \mathbf{E} \partial \mathbf{x}} \cdot \left(\frac{\partial^2 \Phi}{\partial \mathbf{x}^2} \right)^{-1} \frac{\partial^2 \Phi}{\partial \mathbf{x} \partial \mathbf{E}} \right]_{\mathbf{E}=0, \mathbf{x}=0} \quad (3.16)$$

In the following, both cases will be calculated in order to show the effect of inner displacement on the elastic constants at zero strain condition.

Table II. Comparison of calculation and experimental data of C_{11} for graphite

Methods	Results(GPa)	Young's Modulus(GPa)
<i>HomogeneousI^a</i>	1078	1051
<i>HomogeneousII^b</i>	1086	1058
<i>InhomogeneousI^c</i>	837	705
<i>Experiment</i>	1060 ^d	1020 ^e

- a) Calculated by (3.3)
- b) Calculated by (3.11)
- c) Reported by Zhang et al. (2002)
- d) Measured by Fitzer (1989)
- e) Measured by Blakslee et al. (1970)

Table II summarized the results of C_{11} and Young's modulus and the comparison with the experimental data. Young's modulus is calculated as the inverse of the (1, 1) component of the compliance matrix. (a) is the result corresponding to (3.3), which is reasonable because the inner displacement at zero strain is zero. The value is consistent with experimental data. (c) is the result corresponding to (3.16). It is obvious that Zhang's model is not comparable with experimental data. He extended the same methodology to calculate Young's modulus of SWNT, and the result is about 705 *GPa* (no dependence on radius was given in his paper).

The C_{11} and Young's modulus at different strain conditions were also calculated. In these cases, the inner displacement can not be neglected. The inner displacement in the x_2 direction is significant (the value of x_1 is negligible and not given in table III).

The inner displacement is determined by the minimization of potential energy, and potential energy is only the function of strain components. The results of the last two columns in table III were calculated by equation (3.3). It is obvious that the influence of inner displacement on the C_{11} and Young's modulus increases with

Table III. C_{11} and Young's modulus considering the inner displacement and comparison with results from homogeneous deformation

Strain	x_2	C_{11}	E_y	C_{11}^a	E_y^a
0	$1.1375 * 10^{-10}$	1078	1051	1078	1051
0.001	0.000576	1070	1044	1069	1042
0.005	0.002861	1038	1014	1030	1006
0.01	0.00566	999	978	984	962

a) calculated by equation (3.3)

increasing strain.

It is clear from the above calculation that at zero strain both C_{11} and Young's modulus are consistent with experimental data. In the following calculation, we only considered the homogeneous deformation at zero strain condition.

2. New stress deformation behavior

For graphite, at least three lattice vectors $\mathbf{e}_{(i)}$ ($i = 1, 2, 3$) are needed to describe the whole structure (fig. 6).

The lattice vectors $\mathbf{e}_{(1)}$ and $\mathbf{e}_{(2)}$ determine the external structure of the unit cell while $\mathbf{e}_{(3)}$ determines the internal structure.

As introduced in chapter I, the specific Helmholtz free energy \hat{A} can be expressed as a function of temperature and five invariants.

$$\hat{A} = \hat{A}(T, I_{(11)}, I_{(22)}, I_{(12)}, I_{(13)}, I_{(23)}) \quad (3.17)$$

The position of $\mathbf{e}_{(3)}$ is determined by the minimization of potential energy. So the Helmholtz free energy can be expressed only as the function of temperature and three independent invariants.

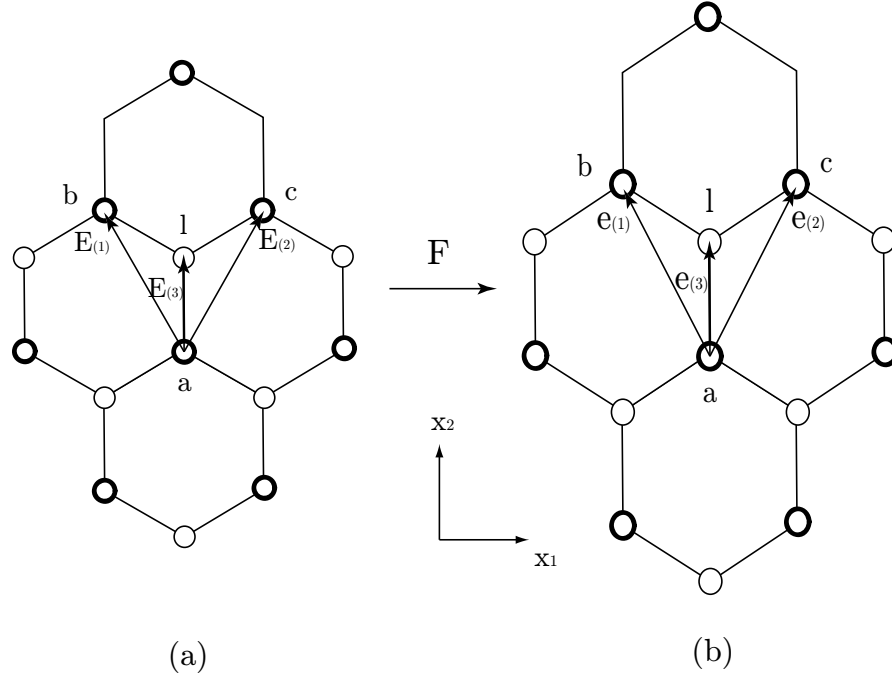


Fig. 6. Schematic of (a) an undeformed and (b) a deformed graphite layer by a homogeneous deformation \mathbf{F} .

$$\hat{A} = \hat{A}(T, I_{(11)}, I_{(12)}, I_{(22)}) \quad (3.18)$$

For an infinitesimal deformation, all distances between atoms which are not covalently bonded are greater than the cutoff distance for the Tersoff - Brenner potential. It means that the strain energy is just the sum of all covalent bond energies. In view of equation (3.4), the Helmholtz free energy in the representative triangle cell $a - b - c$ in fig. 6 becomes

$$\begin{aligned} \Phi &= \Phi_{al} + \Phi_{bl} + \Phi_{cl} \\ &= \Phi(I_{(11)}, I_{(12)}, I_{(22)}) \end{aligned} \quad (3.19)$$

The coefficients in the quadratic state function can be calculated by the second deriv-

ative of total interatomic potential energy with respect to the invariants.

$$\begin{aligned} a_{(ijmn)} &= a_{(mnij)} \\ &= \frac{\partial^2 \Phi}{\partial I_{(ij)} \partial I_{(mn)}} \end{aligned} \quad (3.20)$$

As mentioned in the above section, the equilibrium bond lengths for two sets of parameters are $0.142nm(Coef1)$ and $0.145nm(Coef2)$ respectively by minimizing the potential energy.

The components of the stiffness tensor can be evaluated by the coefficients through equation (3.11). During the calculation, notice that the theory is based on the assumption of specific energy per unit mass, while the interatomic potential gives the energy per unit cell or per unit atom. The results of C_{11} and Young's modulus are $1086 GPa$ and $1058 GPa$ respectively.

E. Single-walled carbon nanotubes

Interest in carbon nanotubes continues to grow since their first discovery (Iijima, 1991). An ideal nanotube can be thought of as a hexagonal network of carbon atoms that has been rolled up to make a seamless cylinder. Three types of nanotubes are possible, and these are called armchair, zigzag and chiral nanotubes, depending on how the two-dimensional graphene sheet is rolled up. If the CNT is free from defects, the elastic properties should be the same as the graphene sheet. However, as shown in the following, the difference is due to the curvature. The properties are the same as the graphene sheet in the limit of a large radius.

There are different ways to define the structure of carbon nanotubes. The most common way is to think of CNT as a result of rolling a graphene sheet, by specifying the direction of rolling and the circumference of the cross section, as shown in fig.7.

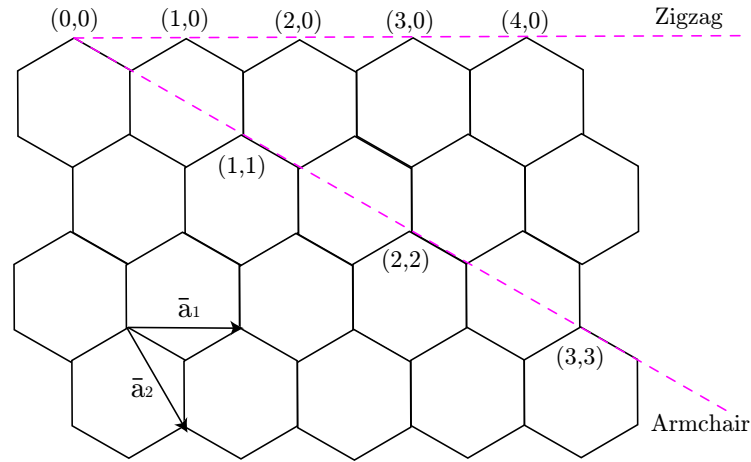


Fig. 7. Definition of roll-up vector as linear combination of base vector \bar{a}_1 and \bar{a}_2

The so-called chiral vector, \mathbf{C}_h , is defined by

$$\mathbf{C}_h \equiv n\bar{a}_1 + m\bar{a}_2 \quad (3.21)$$

where \bar{a}_1 and \bar{a}_2 are unit vectors in 2-D hexagonal lattice, and n and m are integers. *Armchair* nanotubes are formed when $n = m$ and *Zigzag* means either one of them is zero. All others are known as *Chiral* nanotubes. Another important parameter is chiral angle, which is defined as the angle between \mathbf{C}_h and \bar{a}_1 . Chiral angle is 0° and 30° for *Zigzag* and *Armchair*, respectively.

The equilibrium energy and position of atoms will change due to rolling. The strain energy relative to the graphite was given in fig. 8. The change of position of zigzag nanotubes was shown in fig. 9.

Carbon nanotubes may be used as potential reinforcements in nanocomposite materials and other applications due to their superior mechanical properties (Ruoff and Lorents, 1995; Srivastava et al., 2001; Yakobson and Avouris, 2001; Odegard et al., 2002, 2003, 2005a,b). The deformation of Single-Walled Carbon Nanotubes

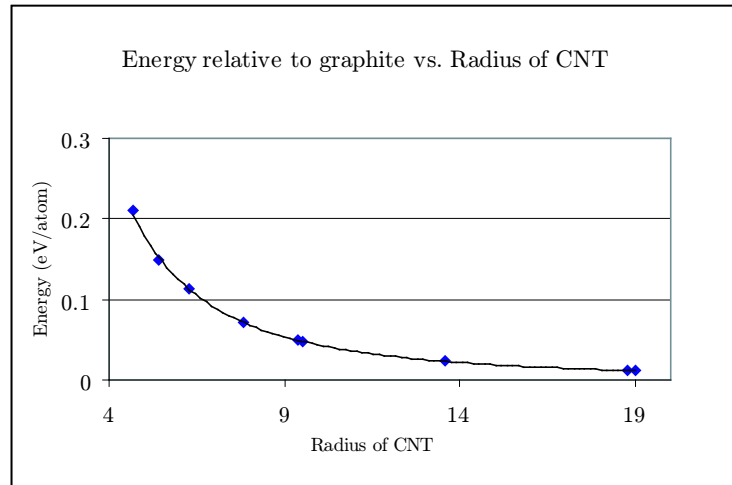


Fig. 8. The strain energy relative to the graphite vs. the radius of SWCNT. Zero energy corresponds to the equilibrium graphite energy of -7.3756 eV/atom

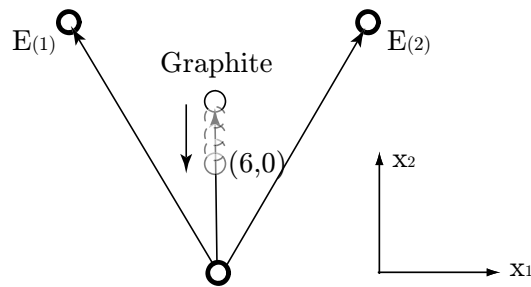


Fig. 9. The equilibrium position of zigzag nanotubes and comparison with graphite (SWNT) is reversible up to strains of more than 4 percent (Iijima et al., 1996; Wong et al., 1997; Lourie and Wagner, 1998; Wagner et al., 1998; Tomblor et al., 2000; Yu et al., 2000a).

The reported elastic modulus of carbon nanotubes from experiments and calculations are summarized in table IV and table V separately.

In the case of SWCNT, the lattice vectors are actually the cords between two atoms on the curved surface. The surface lattice vector is defined as

$$\mathbf{e}_{(i)} \equiv \mathbf{P}\mathbf{e}_{(i)}^p, i = 1, 2, \dots, k \quad (3.22)$$

where \mathbf{P} is the projection vector (Slattery, 1990, pg.1085) and $\mathbf{e}_{(i)}^p$ is the primitive lattice vector.

The extended Cauchy - Born rule to the curved surface proposed by Arroyo and Belytschko (2002) is as follows

$$e_{(i)} \equiv \mathcal{F}E_{(i)} \quad (3.23)$$

where \mathcal{F} is surface deformation gradient.

Oh et al. (2005) assumed the surface Helmholtz free energy is the function of temperature and surface lattice vectors, with the assumption that $e_{(i)}^p \approx e_{(i)}$. They obtained the stress deformation behavior in the limit of infinitesimal deformation at equilibrium state.

$$\mathbf{T}^{(\sigma)} = 2\rho_{\kappa}^{(\sigma)} \sum_{m=1}^2 \sum_{n \geq m}^2 \sum_{i=1}^2 \sum_{j \geq i}^2 a_{(ijmn)} (\mathbf{E}_{(i)} \cdot \boldsymbol{\varepsilon}^{(\sigma)} \mathbf{E}_{(j)}) (\mathbf{E}_{(m)} \otimes \mathbf{E}_{(n)} + \mathbf{E}_{(n)} \otimes \mathbf{E}_{(m)}) \quad (3.24)$$

where superscript σ donates a quantity defined on a surface. Actually, it can be regarded as a special case of equation (2.25).

However, during the calculation of elastic properties of CNT, the same mistake was made as Zhang et al. (2002). The result is around 800GPa in the limit of a large radius, which is not consistent with the experimental data of graphite.

Here, the Young's modulus of CNT was calculated with the assumption of homogeneous deformation. The C_{11} and Young's modulus of both Zigzag and Armchair carbon nanotubes were calculated using equation (3.24). The results are shown in figures 10, 11, 12, which fall in the range of previous reports by most experimental

Table IV. Reported elastic modulus of SWNT from experiment

Author(Year)	Method	Result(TPa)
Treacy et al. (1996)	<i>TEM</i>	0.4–4.15
Wong et al. (1997)	<i>AFM</i>	0.69–1.87
Krishnan et al. (1998)	<i>TEM</i>	0.9–1.7
Muster et al. (1998)	<i>SFM</i>	1
Pan et al. (1999)	Nanoscale tensile test	0.22–0.68
Yu et al. (2000b)	Nanoscale tensile test	0.32–1.47
Salvetat et al. (1999)	<i>AFM</i>	0.6
Tomblor et al. (2000)	<i>AFM</i>	1.2

Table V. Reported elastic modulus of SWNT from calculation

Author(Year)	Method	Result(TPa)
Yakobson et al. (1996)	Molecular Dynamics	1.07
Cornwell and Wille (1997)	TB Potential	0.8
Overney et al. (1993)	Keating Potential	1.5
Lu (1997)	Keating Potential	0.97
Hernandez et al. (1998)	Tight Binding	1.2
Yao and Lordi (1998)	Molecular Dynamics	1
Yu et al. (2000a)	Keating Potential	1.1–1.2
Popov et al. (2000)	Lattice Dynamics	1
Zhou et al. (2001)	Electronic Band Theory	0.76
Zhang et al. (2002)	TB Potential	0.7
Oh et al. (2005)	TB Potential	0.8

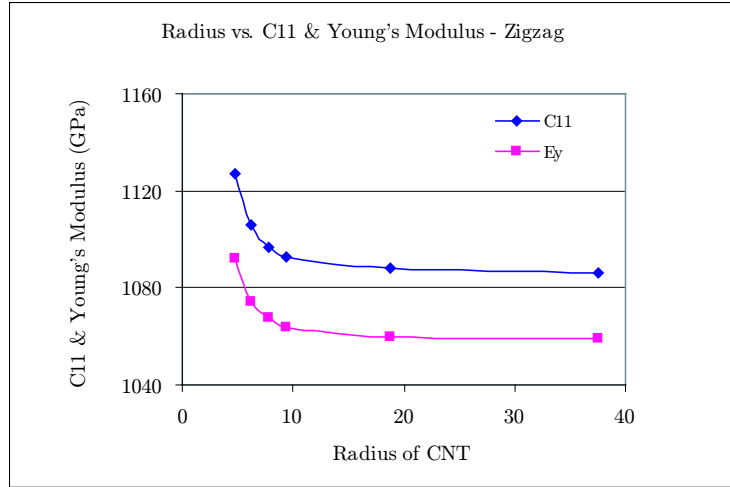


Fig. 10. The relationship between the radius of CNT and C_{11} , Young's modulus of zigzag CNT

and calculation studies of SWCNTs (Hernandez et al. (1998); Krishnan et al. (1998); Wong et al. (1997); Tombler et al. (2000); Overney et al. (1993); Yu et al. (2000a,b); Popov et al. (2000)).

Yao and Lordi (1998) used MD simulation and showed the same trend (fig. 11) of dependence of Young's modulus on the radius. Fig. 12 showed that chirality has little effect on Young's modulus especially for the CNT with a radius over 5 \AA (Lu, 1997). Oh et al. (2005) showed a different trend for armchair nanotubes.

Table VI showed the results corresponding to different conditions.

F. Discussion

From the above calculations, we concluded that homogeneous deformation is a good assumption at zero strain, considering the inner displacement at zero strain condition will lead to incorrect results. In the case of non-zero strain condition, the inner displacement can not be neglected, but should be minimized out of the energy function.

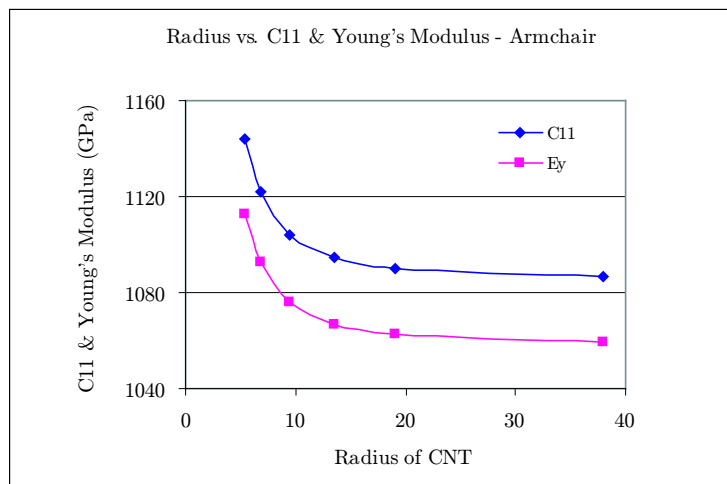


Fig. 11. The relationship between the radius of CNT and C_{11} , Young's modulus of armchair SWCNT

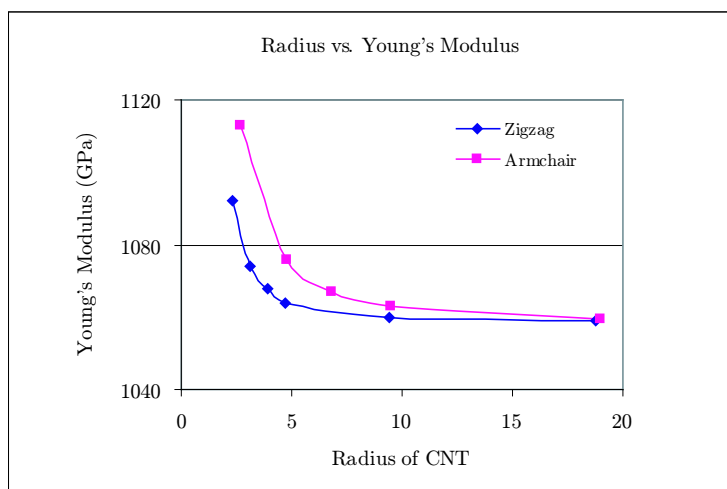


Fig. 12. The relationship between the radius of CNT and Young's modulus

Table VI. Comparison of C_{11} and Young's modulus at different strain conditions - zigzag

Zigzag	C_{11}^a	E_y^a	C_{11}^b	E_y^b	C_{11}^c	E_y^c
(6, 0)	1127	1092	1124	1092	1110	1078
(8, 0)	1106	1074	1114	1076	1101	1063
(10, 0)	1097	1068	1099	1068	1094	1065
(12, 0)	1093	1064	1094	1065	1081	1051
(24, 0)	1088	1060	1073	1042	1055	1028

- a) zero strain homogeneous deformation
- b) 0.005 homogeneous deformation
- c) 0.005 considering inner displacement

The problem with Zhang's methodology is taking the inner displacement into account at zero strain, while considering energy as a function of the shift vector. The lattice vectors in equation (1.1) are skeletal lattice vectors.

This method also can be extended to calculate Young's modulus of multi-walled carbon nanotubes. Kiang et al. (1998) have shown the interspacing for MWCNTs changes from 3.4 Å to 3.75 Å. Using this information, we can visualize that Young's modulus might be lower than that of SWCNTs (Wagner et al., 1998; Yu et al., 2000b).

CHAPTER IV

ELASTIC PROPERTIES OF DIAMOND AND SILICON

A. Structure of diamond and silicon

The electronic configuration of carbon is $1s^2 2s^2 2p^2$, i.e., four valence electrons spread in the s and p orbitals. In order to create covalent bonds in a diamond, the s orbital mixes with the three p orbitals to form sp^3 hybridization. The four valence electrons are distributed equally among the sp^3 orbitals. The tetrahedral structure gives strength and stability to the bonds. Consequently, all the bonds in diamonds are of the same length (1.54 Å), as shown in fig. 13, with the same bond angle of 109.47° .

The structure of a diamond unit cell is given in fig. 14. It can be viewed as the interpenetration of two fcc lattices, each displaced $1/4$ of a lattice constant in each direction from the other. Let A denote the sublattice corresponding to the green circles and B represent the sublattice with purple circles. As shown in fig.14, the atom l belonging to the B sublattice connected with four atoms in the A sublattice. Examples of materials with the diamond crystal structure are diamond, silicon and germanium.

In the case of diamonds, whose structure can not be fully described only by basis lattice vectors, a shift vector \mathbf{p}_k defined in chapter III was needed to interpret the configuration of crystal structure. However, according to the discussion above, in the case of graphite and SWCNT, \mathbf{p}_k is not included in the energy function and the equilibrium condition was used to determine this shift vector (Ericksen, 1984; Zanzotto, 1996).

As shown in the following section, the potential energy is only the function of

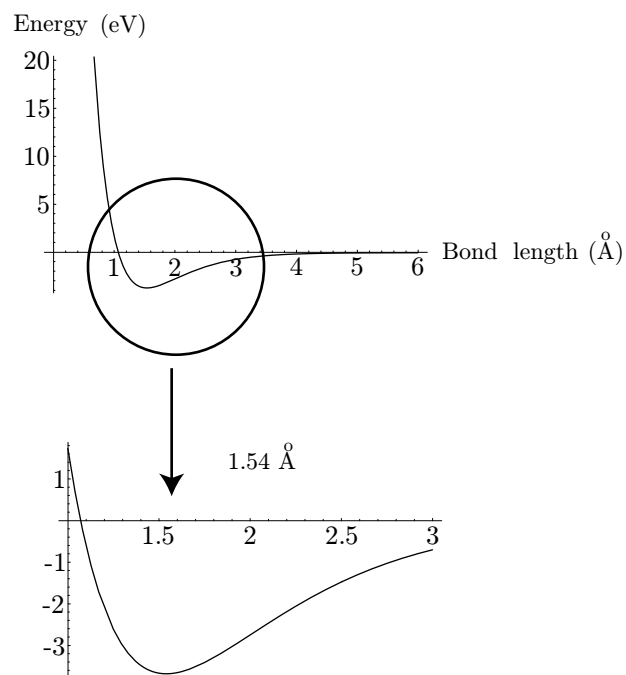


Fig. 13. Interatomic potential energy vs. distance between atoms - diamond

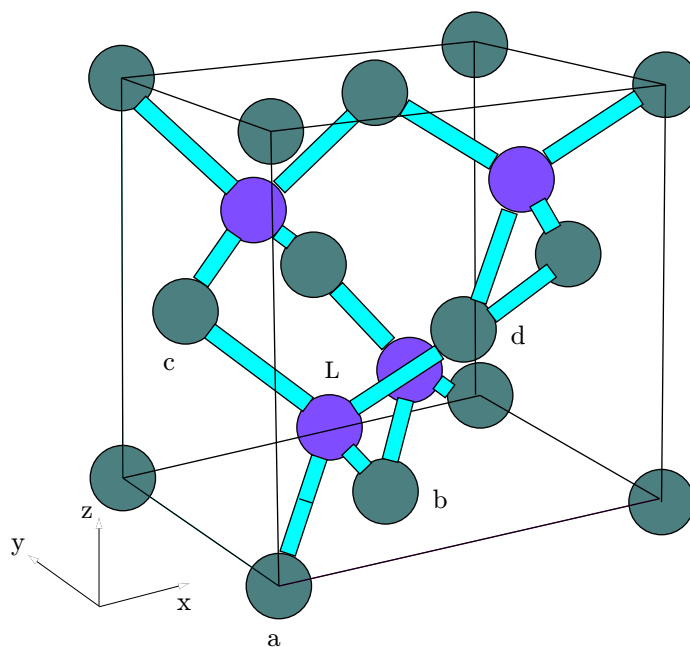


Fig. 14. Structure of diamond unit cell. The green and purple circles represent the atoms on the two different sublattices

six invariants (without the Cauchy - Born rule , the energy should be the function of ten invariants,i.e., six invariants plus $I_{(14)},I_{(24)},I_{(34)},I_{(44)}$). The result of energy minimization is consistent with the assumption of homogenous deformation. The relative position of the shift vector does not change during the deformation, which means there is no relative shift during the deformation.

In order to use the Tersoff - Brenner potential to describe the potential energy in the representative cell, the distances between atoms during the deformation should be expressed as a function of deformed lattice vectors $\mathbf{e}_{(1)},\mathbf{e}_{(2)}$ and $\mathbf{e}_{(3)}$.

$$\begin{aligned}
|ab| &= |\mathbf{e}_{(1)} + \mathbf{e}_{(2)}| \\
|ac| &= |\mathbf{e}_{(2)} + \mathbf{e}_{(3)}| \\
|ad| &= |\mathbf{e}_{(3)} + \mathbf{e}_{(1)}| \\
|al| &= \left| \frac{1}{2}(\mathbf{e}_{(1)} + \mathbf{e}_{(2)} + \mathbf{e}_{(3)}) \right| \\
&\dots \\
|bc| &= |\vec{a}\vec{c} - \vec{a}\vec{b}| \\
&\dots
\end{aligned} \tag{4.1}$$

B. Elastic properties of diamond

In the superelastic model, the strain energy is given

$$\begin{aligned}
\phi &= \frac{1}{2}T_{ij}\varepsilon_{ij} \\
&= \frac{1}{2}C_{ijkl}\varepsilon_{ij}\varepsilon_{kl}
\end{aligned} \tag{4.2}$$

For cubic systems, the stress in terms of stiffness tensor and strain is given

$$\begin{aligned}
T_{11} &= C_{11}\varepsilon_{11} + C_{12}\varepsilon_{22} + C_{12}\varepsilon_{33} \\
T_{22} &= C_{12}\varepsilon_{11} + C_{11}\varepsilon_{22} + C_{12}\varepsilon_{33} \\
T_{33} &= C_{12}\varepsilon_{11} + C_{12}\varepsilon_{22} + C_{11}\varepsilon_{33} \\
T_{23} &= 2C_{44}\varepsilon_{23} \\
T_{13} &= 2C_{44}\varepsilon_{13} \\
T_{12} &= 2C_{44}\varepsilon_{12}
\end{aligned} \tag{4.3}$$

There are two ways to calculate the stiffness tensor. One is given by

$$C_{ijkl} = \frac{\partial^2 \phi}{\partial \varepsilon_{ij} \partial \varepsilon_{kl}} \tag{4.4}$$

The other is to introduce three kinds of deformation for each component. For C_{11} , we assume a strain with only one non zero component $\varepsilon_{11} = \varepsilon$.

$$C_{11} = 2 \frac{\Delta \phi}{\varepsilon^2} \tag{4.5}$$

Similarly C_{44} can be determined by applying a strain with only one non zero component $\varepsilon_{23} = \varepsilon$.

$$C_{44} = \frac{\Delta \phi}{\varepsilon^2} \tag{4.6}$$

C_{12} can be calculated by

$$E_y = \frac{(C_{11} + 2C_{12}) \cdot (C_{11} - C_{12})}{C_{11} + C_{12}} \tag{4.7}$$

or we can assume another form of strain. For example, $\varepsilon_{11} = -\varepsilon_{22} \neq 0$ for $C_{11} - C_{12}$. We can obtain C_{12} with C_{11} from equation (4.5).

Young's modulus is the slope of the linear part of stress vs. strain curve. The

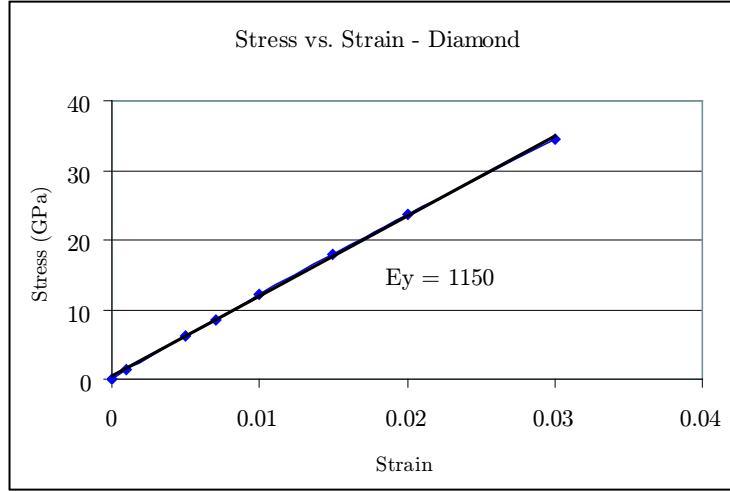


Fig. 15. Young's modulus of diamond determined through stress strain curve

Table VII. Inter displacement between two fcc sublattices under different axial strain conditions - diamond

Strain	x	y	z
<i>Zerostrain</i>	$-5.368 * 10^{-11}$	$-5.368 * 10^{-11}$	$-5.368 * 10^{-11}$
0.001	$-3.857 * 10^{-11}$	$-9.983 * 10^{-11}$	$-9.983 * 10^{-11}$
0.005	$1.534 * 10^{-9}$	$-8.610 * 10^{-10}$	$-8.610 * 10^{-10}$
0.01	$5.619 * 10^{-9}$	$-2.987 * 10^{-9}$	$-2.987 * 10^{-9}$
0.02	$-7.475 * 10^{-14}$	$-6.604 * 10^{-13}$	$-6.604 * 10^{-13}$

result is shown in fig. 15.

Table VII shows the inner displacement between the two fcc sublattices. It is obvious that homogeneous deformation is a good assumption even at non-zero strain conditions. The position of L was determined by the minimization of potential energy. The density of diamond in the reference configuration used in the calculation is $3.544g/cm^3$ corresponding to the equilibrium bond length 1.54\AA .

In this study, we calculated stiffness tensor according to equation (4.5) while choosing $\varepsilon = 0.03$. The results are given in table VIII.

In order to calculate the coefficients in the quadratic state function, the scalar product of deformed lattice vectors were expressed in terms of invariants.

$$\begin{aligned}
\mathbf{e}_{(1)} \cdot \mathbf{e}_{(1)} &= I_{(11)} + \mathbf{E}_{(1)} \cdot \mathbf{E}_{(1)} \\
\mathbf{e}_{(2)} \cdot \mathbf{e}_{(2)} &= I_{(22)} + \mathbf{E}_{(2)} \cdot \mathbf{E}_{(2)} \\
\mathbf{e}_{(3)} \cdot \mathbf{e}_{(3)} &= I_{(33)} + \mathbf{E}_{(3)} \cdot \mathbf{E}_{(3)} \\
\mathbf{e}_{(1)} \cdot \mathbf{e}_{(2)} &= I_{(12)} + \mathbf{E}_{(1)} \cdot \mathbf{E}_{(2)} \\
\mathbf{e}_{(2)} \cdot \mathbf{e}_{(3)} &= I_{(23)} + \mathbf{E}_{(2)} \cdot \mathbf{E}_{(3)} \\
\mathbf{e}_{(3)} \cdot \mathbf{e}_{(1)} &= I_{(31)} + \mathbf{E}_{(3)} \cdot \mathbf{E}_{(1)}
\end{aligned} \tag{4.8}$$

Using the second cosine law (4.9), the bond angles can be expressed in terms of bond lengths, which is also a function of invariants. Now all terms in the Tersoff - Brenner potential are represented in terms of invariants and parameters.

$$\theta_{lab} = \arccos\left(\frac{r_{al}^2 + r_{bl}^2 - r_{ab}^2}{2r_{al}r_{bl}}\right) \tag{4.9}$$

The unit of coefficients in the quadratic state function $a_{(ijmn)}$ is $eV/g \cdot \text{\AA}^4$ ($1eV = 1.6 * 10^{-19} N \cdot m$)

The stored energy in the diamond cell is just the sum of all covalent bond energies. The Helmholtz free energy in the representative cell is

$$\begin{aligned}
\hat{A} &= \Phi_{al} + \Phi_{bl} + \Phi_{cl} + constant \\
&\equiv \Phi(I_{(11)}, I_{(22)}, I_{(33)}, I_{(12)}, I_{(13)}, I_{(23)}) + constant
\end{aligned} \tag{4.10}$$

The results of coefficients in the state function for diamond are

Table VIII. Elastic properties of diamond(GPa)

	Our model	Superelastic	<i>Experiment</i> ^(a)
C_{11}	1071	1061	1015 ± 65
C_{12}	223	229	225 ± 100
C_{44}	603	638	500 ± 75

(a) measured by Ownby and Stewart (1991)

$$\begin{aligned}
 a_{(1111)} &= a_{(2222)} = a_{(3333)} = 7560 \\
 a_{(1122)} &= a_{(2233)} = a_{(3311)} = 1274 \\
 a_{(1212)} &= a_{(2323)} = a_{(1313)} = 4141
 \end{aligned}
 \tag{4.11}$$

Table VIII summarized the results from calculations and experiments.

C. Elastic properties of silicon

1. Potential function for silicon bond

Tersoff (1988b) gave an interatomic potential form for silicon systems, which is basically the same form as the Tersoff - Brenner potential for carbon-carbon bonds(Tersoff, 1988a; Brenner, 1990b).

$$\Phi_{ij} = f_c(r_{ij})[a_{ij}f_R(r_{ij}) + b_{ij}f_A(r_{ij})]
 \tag{4.12}$$

where $f_R(r_{ij})$ and $f_A(r_{ij})$ are the repulsive and attractive terms

$$\begin{aligned}
 f_R(r_{ij}) &= Aexp[-\lambda_1 r_{ij}] \\
 f_A(r_{ij}) &= -Bexp[-\lambda_2 r_{ij}]
 \end{aligned}
 \tag{4.13}$$

and $f_c(r_{ij})$ is the cutoff function

$$f_c(r_{ij}) = \begin{cases} 1, & r_{ij} < R - D; \\ \frac{1}{2} - \frac{1}{2}(\cos[\frac{\pi}{2}(r - R)/D]), & R - D < r_{ij} < R + D; \\ 0, & r_{ij} > R + D. \end{cases} \quad (4.14)$$

Bond order factor b_{ij} is given by

$$b_{ij} = (1 + \beta^n \xi_{ij}^n)^{-1/2n} \quad (4.15)$$

where

$$\begin{aligned} \xi_{ij} &= \sum_{k(\neq i,j)} f_c(r_{ik})g(\theta_{ijk})\exp[\lambda_3^3(r_{ij} - r_{ik})^3] \\ g(\theta) &= 1 + c^2/d^2 - c^2/[d^2 + (h - \cos[\theta]^2)] \\ a_{ij} &= (1 + \alpha^n \eta^n)^{-1/2n} \\ \eta_{ij} &= \sum_{k \neq i,j} \exp[\lambda_3^3(r_{ij} - r_{ik})^3] \end{aligned} \quad (4.16)$$

All parameters in the above equations are given in table IX.

It is obvious that the coefficient a_{ij} is zero. The relationship between the potential energy and bond length was given in fig. 16.

2. Elastic properties of silicon

Silicon has the same structure as diamond. Table X shows the inner displacement between two fcc sublattices under different axial strain conditions.

The results of coefficients in the state function (1.16) of silicon are

Table IX. Parameters of Tersoff potential for silicon bonds

	Coef
$A(eV)$	1.8308×10^3
$B(eV)$	4.7118×10^2
$\lambda_1(\text{\AA}_{-1})$	2.4799
$\lambda_2(\text{\AA}_{-1})$	1.7322
α	0
β	1.0999×10^{-6}
n	7.8734×10^{-1}
c	1.0039×10^5
d	1.6218×10^1
h	-5.9826×10^{-1}
$\lambda_3(\text{\AA}^{-1})$	1.7322
$R(\text{\AA})$	2.85
$D(\text{\AA})$	0.15

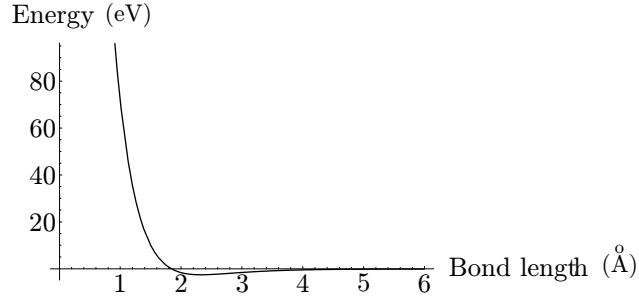


Fig. 16. Potential energy vs. bond length - silicon

Table X. Inner displacement between two fcc sublattices under different axial strain conditions - silicon

Strain	x_1	x_2	x_3
<i>Zerostrain</i>	-1.064×10^{-11}	-1.064×10^{-11}	-1.064×10^{-11}
0.001	-2.920×10^{-8}	9.010×10^{-8}	9.010×10^{-8}
0.005	8.335×10^{-10}	-4.382×10^{-10}	-4.382×10^{-10}
0.01	2.975×10^{-9}	-1.540×10^{-9}	-1.540×10^{-9}
0.02	-8.584×10^{-14}	-7.758×10^{-14}	-7.758×10^{-14}

Table XI. Elastic properties of silicon(GPa)

	Our model	<i>Superelastic</i> ^(a)	<i>Experiment</i> ^(b)
C_{11}	142	142	166.6
C_{12}	66.3	67.6	64
C_{44}	59	59	79.6

(a) calculated by Balamane et al. (1992)

(b) measured by Simmons and Wang (1971)

$$\begin{aligned}
 a_{(1111)} &= a_{(2222)} = a_{(3333)} = 2762 \\
 a_{(1122)} &= a_{(2233)} = a_{(3311)} = 1451 \\
 a_{(1212)} &= a_{(2323)} = a_{(1313)} = 1359
 \end{aligned} \tag{4.17}$$

The density of silicon in the reference configuration is $2.3322g/cm^3$, corresponding to equilibrium bond length 2.35212\AA , as shown in fig.16.

Table XI summarized the results from calculation and the comparison with experiment results. The calculated result of C_{44} is not consistent with experimental data even though this Tersoff potential was supposed to give a better description of elastic properties than the old version (Tersoff, 1988a). It is obvious that the difference between the calculated results and experimental data is due to the accuracy of the potential function rather than this new stress deformation behavior.

CHAPTER V

ELASTIC PROPERTIES OF VANADIUM

Finnis and Sinclair (1984) potential (hereafter referred to as FS) is a short range, many body empirical potential. The corresponding long range form was given by Sutton and Chen (1990).

The FS potential has the following form

$$\Phi = \Phi_1 + \Phi_2 = \frac{1}{2} \sum_{i,j:i \neq j}^N V_1(r_{ij}) + \sum_{i=1}^N V_2(n_i) \quad (5.1)$$

where

$$V_1(r_{ij}) = \left(\frac{a}{r_{ij}} \right)^n \quad (5.2)$$

$$V_2(n_i) = -A\sqrt{n_i} \quad (5.3)$$

n_i is the local electronic charge density.

$$n_i = \sum_{i:i \neq j}^N \Phi(r_{ij}) \quad (5.4)$$

The function $\Phi(r_{ij})$ is given by:

$$\Phi(r_{ij}) = \begin{cases} (r_{ij} - d)^2, & r_{ij} < d; \\ 0, & r_{ij} > d. \end{cases} \quad (5.5)$$

$V_1(r_{ij})$ is a pairwise potential representing repulsive interactions.

$$\Phi(r_{ij}) = \begin{cases} (r_{ij} - c)^2(c_0 + c_1 r_{ij} + c_2 r_{ij}^2), & r_{ij} \leq c; \\ 0, & r_{ij} > c. \end{cases} \quad (5.6)$$

Table XII. Parameters of FS potential of vanadium

Parameters	<i>Value</i> ^(a)
A	2.010637 eV
d	3.692767 Å
c	3.8 Å
c_0	-0.8816318
c_1	1.4907756
c_2	-0.397637

(a) fit to Finnis and Sinclair (1984)

Table XIII. Elastic constants of vanadium by FS potential

	Experiment	Superelastic	This study
C_{11}	2.279	2.27607	2.27565
C_{12}	1.187	1.18548	1.18546
C_{44}	0.426	0.42545	0.42542

A , d , c , c_0 , c_1 and c_2 are the fitting parameters.

For Vanadium, which has a bcc structure, the values of those six parameters were given in table XII.

All parameters were fitted with the lattice constant, bulk modulus, cohesive energy and three elastic constants. It's not surprising that this potential is capable of reproducing the elastic constants correctly.

We used this potential to calculate the elastic constants. The results are almost exactly the same as the superelastic model and the experimental data (Table XIII).

CHAPTER VI

CONCLUSIONS

One of the most important new implications of equilibrium is the stress–deformation behavior in the equilibrium state. This new stress expression is an explicit function of the deformed lattice vectors.

In the limit of infinitesimal deformations, the specific Helmholtz free energy can be represented as a quadratic function of the invariants $I_{(mn)}$. The coefficients in this quadratic function can be determined for a given interatomic potential. The elastic properties of graphite, single wall carbon nanotubes, diamond, silicon and vanadium were calculated. A few successful applications of the new stress deformation behavior were shown in this thesis:

1. We calculated the Young’s modulus of graphite and the results are consistent with the experimental data. We have shown that homogeneous deformation is a good assumption at zero strain. Inappropriate consideration of inner displacement will lead to incorrect results. For non zero strain, the inner displacement should be determined by minimization of potential energy. The chirality has little effect on the Young’s modulus of SWCNT.

2. The stiffness tensor and Young’s modulus of diamond and silicon were calculated with the Tersoff - Brenner potential and the Tersoff potential respectively. The results are consistent with the superelastic model. The difference of C_{44} between the calculated results and the experimental data was due to the accuracy of the potential energy function.

3. Using FS potential for metals, the stiffness tensor of vanadium was calculated, and the result was almost the same as the experimental data since the parameters of this potential were fitted to elastic constants.

From this study, we have shown that one effective approach is to use this new stress expression in the limit of infinitesimal deformations. This study can be regarded as a support for the theory introduced in Slattery and Lagoudas (2005).

We also recognized the limitation of this approach in using the new stress expression. It is apparently dependent on the available potential functions.

NOTATION

Roman Symbols

a_0	parameter in Tersoff - Brenner potential
$a_{(ijmn)}$	defined by equation (1.9)
\hat{A}	Helmholtz free energy per unit mass
\check{A}	Helmholtz free energy per unit volume
\mathbf{b}	body force per unit mass
c_0	parameter in Tersoff - Brenner potential
\mathbf{C}	right Cauchy–Green strain tensor
c_0	parameter in Tersoff - Brenner potential
C_h	chiral vector given by (3.21)
C_{ijmn}	Stiffness component
d_0	cut off distance in Tersoff - Brenner potential
D^e	parameter in Tersoff - Brenner potential
$\mathbf{e}_{(i)}$	surface lattice vectors in the deformed configuration
\mathbf{E}	the lagrangian strain tensor
\hat{E}	sum of internal energy and kinetic energy per unit mass as defined by (2.17)
$\mathbf{E}_{(i)}$	surface lattice vectors in the reference configuration
\mathbf{F}	deformation gradient
$I_{(mn)}$	scalar invariants defined by equation (1.5)
l_0	equilibrium bond length
P	thermodynamic pressure
\mathbf{p}_k	shift vector given by equation (1.30)

R^e	parameter in Tersoff - Brenner potential
S	parameter in Tersoff - Brenner potential
\hat{S}	entropy per unit mass
t	time
\mathbf{T}	Stress tensor
\hat{U}	internal energy per unit mass
\hat{V}	volume per unit mass
Z_A	defined by (2.11)
Z_e	defined by (2.16)
\mathbf{Z}_m	defined by (2.13)

Greek letters

β	parameter in Tersoff - Brenner potential
δ	parameter in Tersoff - Brenner potential
ϵ	Strain tensor
λ_A	Lagrangian multiplier
λ_e	Lagrangian multiplier
λ_m	Lagrangian multiplier
$\mu_{(I,mn)}$	defined by equation (1.18)
ξ	unit normal to phase interface
σ	phase interface
ρ	overall mass density
Φ	interatomic potential energy
$\omega_{(A)}$	mass fraction of species A or $\rho_{(A)}/\rho$

Other

dA indicates that an area integration should be performed

dV indicates that a volume integration should be performed.

The integrand will be discontinuous generally at phase interfaces.

$\frac{d_{(v)}}{dt}$ derivative following a particle that moves with the mass-averaged velocity \mathbf{v}

$\frac{d_{(s)}}{dt}$ derivative following a surface material particle that moves with the surface velocity $\mathbf{v}^{(\sigma)}$

REFERENCES

- Abell, G. C., 1985. Empirical chemical pseudopotential theory of molecular and metallic bonding. *Physical Review B* 31, 6184.
- Arroyo, M., Belytschko, T., 2002. An atomistic based finite deformation membrane for single layer crystalline films. *Journal of the Mechanics and Physics of Solids* 50, 1941–1977.
- Balamane, H., Halicioglu, T., Tiller, W. A., 1992. Comparative study of silicon empirical interatomic potentials. *Physical Review B* 46, 2250–2279.
- Barron, T. H. K., Gibbons, T. G., Munn, R. W., 1971. Thermodynamics of internal strain in perfect crystals. *J. Phys. C: Solid St. Phys.* 4, 2805–2821.
- Belytschko, T., Liu, W. K., Moran, B., 2000. *Nonlinear Finite Elements for Continua and Structures*. John Wiley and Sons, Milton, Australia.
- Belytschko, T., Xiao, S. P., Schatz, G. C., Ruoff, R. S., 2002. Atomistic simulations of nanotube fracture. *Physical Review B* 65, 235430–234438.
- Blakslee, O. L., Proctor, D. G., Selden, E. J., Spence, G. B., Weng, T., 1970. Elastic constants of compression-annealed pyrolytic graphite. *J. Appl. Phys.* 41, 3373–3382.
- Born, M., 1915. *Dynamik der Kristallgitter*. B. G. Teubner, leipzig-Berlin.
- Born, M., Huang, K., 1954. *Dynamical Theory of Crystal Lattices*. Clarendon Press, Oxford.
- Brenner, D. W., 1990a. Atomic scale calculations in materials science. *Materials Society Symposia Proceedings* 141, 59.

- Brenner, D. W., 1990b. Empirical potential for hydrocarbons for use in simulating the chemical vapor deposition of diamond films. *Physical Review B* 42, 9458–9471.
- Brugger, K., 1964. Thermodynamic definition of higher order elastic coefficients. *Physical Review* 133(6A), A1611.
- Catlow, C. R. A., Mackrodt, W. C., 1982. *Computer Simulation of Solids*. Springer, New York.
- Cauchy, A. L., 1828. Sur l'équilibre et le mouvement d'un système de points matériels sollicités par forces d'attraction ou de répulsion mutuelle. *Ex. Math.* 3, 227–287.
- Cornwell, C. F., Wille, L. T., 1997. Elastic properties of single-walled carbon nanotubes in compression. *Solid State Communications* 101, 706–709.
- Cousins, C. S. G., 1978. Inner elasticity. *Journal of Physics C* 11, 4867–4879.
- Daw, M. S., Baskes, M. I., 1984. Embedded-atom method: Derivation and application to impurities, surfaces, and other defects in metals. *Physical Review B* 29, 6443.
- Denbigh, K. G., 1963. *The Principles of Chemical Equilibrium*. Cambridge, London.
- Ericksen, J. L., 1980. Some phase transitions in crystals. *Arch. Ration. Mech. Anal.* 73, 99–124.
- Ericksen, J. L., 1984. The Cauchy and Born hypotheses for crystals. In: Curtin, M. E. (Ed.), *Phase Transformations and Material Instabilities in Solids*. Academic Press, New York.
- Finnis, M. W., Sinclair, J. E., 1984. A simple empirical n body potential for transition metals. *Philosophical Magazine A* 50, 45–55.

- Fitzer, E., 1989. Pan-based carbon fibers present state and trend of the technology from the viewpoint of possibilities and limits to influence and to control the fiber properties by the process parameters. *Carbon* 27, 621–645.
- Hernandez, E., Goze, G., Bernier, P., Rubio, A., 1998. Elastic properties of c and bxcynz composite nanotubes. *Phys. Rev. Lett.* 80, 4502–4505.
- Hill, T. L., 1962. *An Introduction to Statistical Thermodynamics*. Addison Wesley, London.
- Hirschfelder, J. O., Curtiss, C., Bird, R. B., 1954. *Molecular Theory of Gases and Liquids*. Wesley, New York.
- Iijima, S., 1991. Helical microtubes of graphitic carbon. *Nature* 354, 56–58.
- Iijima, S., Brabec, C., Maiti, A., Bernholc, J., 1996. Structural flexibility of carbon nanotubes. *Journal of Chemical Physics* 104, 2089–2092.
- James, R. D., 1987. *The Stability and Metastability of Quartz in Metastability and in Completely Posed Problems*. Springer, New York.
- James, R. D., Hane, K. F., 2000. Martensitic transformations and shape memory materials. *Acta Materialia* 48, 197–222.
- Kane, E. O., 1952. A number of potentials which describe bulk phonons of zincblende structure semiconductors. *Physical Review B* 31, 7865.
- Keating, P. N., 1968. Relationship between the macroscopic microscopic theory of crystal elasticity. ii. nonprimitive crystals. *Phys. Review* 169, 758–766.
- Kiang, G. H., Endo, M., Ajayan, P. M., Dresselhaus, G., Dresselhaus, M. S., 1998. Size effects in carbon nanotubes. *Phys. Rev. Lett.* 81, 1869–1872.

- Krishnan, A., Dujardin, E., Ebbesen, T. W., Yianilos, P. N., Treacy, M. M. J., 1998. Young's modulus of single-walled nanotubes. *Physical Review B* 58, 14013–14019.
- Lourie, O., Wagner, H. D., 1998. Evaluation of Young's modulus of carbon nanotubes by micro-raman spectroscopy. *Journal of Materials Research* 13, 2418–2422.
- Lu, J. P., 1997. Elastic properties of carbon nanotubes and nanoropes. *Physical Review Letters* 79, 1297–1300.
- Martin, J. W., 1975a. Many-body forces in metals and Brugger elastic constants. *Journal of Physics C* 8(18), 2837–2857.
- Martin, J. W., 1975b. Many-body forces in solids - elastic constants of diamond type crystals. *Journal of Physics C* 8(18), 2869–2888.
- Martin, J. W., 1975c. Many-body forces in solids and Brugger elastic constants 2 inner elastic constants. *Journal of Physics C* 8(18), 2858–2868.
- Muster, J., Burghard, M., Roth, S., Duesberg, G. S., Hernandez, E., Rubio, A., 1998. Scanning force microscopy characterization of individual carbon nanotubes one-electrode arrays. *Journal of Vacuum Science and Technology B* 16, 2796–2801.
- Odegard, G. M., Clancy, T. C., Gates, T. C., 2005a. Modelling of the mechanical properties of nanoparticle polymer composites. *Polymer* 46, 553–562.
- Odegard, G. M., Gates, T. S., Nicholson, L. M., Wise, K. E., 2002. Equivalent continuum modeling of nano-structured materials. *Composite Science and Technology* 62, 1869–1880.
- Odegard, G. M., Gates, T. S., Wise, K. E., Park, C., Siochi, E. J., 2003. Constitutive modeling of nanotube reinforced polymer composites. *Composite Science and Technology* 63, 1671–1687.

- Odegard, G. M., Pipes, R. B., Hubert, P., 2005b. Comparison of two models of swcn polymer composites. *Composite Science and Technology* 64, 1011–1020.
- Oh, E. S., Lagoudas, D. C., Slattery, J., 2005. Thermodynamics of two-dimensional single-component, elastic, crystalline solids: Single-wall carbon nanotubes. Submitted to *Mechanics of Materials*.
- Overney, G., Zhong, W., Tomanek, D., 1993. Structural rigidity and low-frequency vibrational modes of long carbon tubules. *Zeitschrift für Physik D: Atoms, Molecules and Clusters* 27, 93–96.
- Ownby, P. D., Stewart, R. W., 1991. Engineering properties of diamond and graphite. *Engineered Materials Handbook* 4, 821–834.
- Pan, Z. W., Xie, S. S., Lu, L., Change, B. H., Sun, L. F., Zhou, W. Y., Wang, G., Zhang, D. L., 1999. Tensile tests of ropes of very long aligned multiwall carbon nanotubes. *Applied Physical Letters* 74, 3152–3154.
- Parry, G. P., 1981. On phase transitions involving internal strain. *Int. J. Solids Structures* 17, 361–378.
- Popov, V. N., Doren, V. E. V., m. Balkanski, 2000. Elastic properties of single-walled carbon nanotubes. *Physical Review B* 61, 3078–3084.
- Ruoff, R. S., Lorents, D. C., 1995. Mechanical and thermal properties of carbon nanotubes. *Carbon* 33, 925–930.
- Salvetat, J. P., Briggs, G. A. D., Bonard, J. M., Bascsa, R. R., Kulik, A. J., 1999. Elastic and shear moduli of single-walled carbon nanotube ropes. *Physical Review Letter* 82, 944–947.

- Simmons, G., Wang, H., 1971. *Single Crystal Elastic Constants and Calculated Aggregate Properties*, 2nd Edition. The MIT Press, Cambridge.
- Slattery, J. C., 1990. *Interfacial Transport Phenomena*. Springer-Verlag, New York.
- Slattery, J. C., 1999. *Advanced Transport Phenomena*. Cambridge University Press, Cambridge.
- Slattery, J. C., Lagoudas, D. C., 2005. Thermodynamics of multicomponent, elastic, crystalline solids. *Mechanics of Materials* 37, 121–141.
- Srivastava, D., Menon, M., Cho, K., 2001. Computational nanotechnology with carbon nanotubes and fullerenes. *Computing in Science and Engineering* 3, 42–55.
- Stillinger, F., Weber, T. A., 1985. Computer simulation of local order in condensed phases of silicon. *Physical Review B* 31, 5262–5271.
- Sutton, A. P., Chen, J., 1990. Long range Finnis Sinclair potentials. *Philosophical Magazine Letters* 61, 139–146.
- Tadmor, E. B., Ortiz, M., Phillips, R., 1996. Quasicontinuum analysis of defects in solids. *Philosophy Magazine A* 73, 1529–1563.
- Tersoff, J., 1988a. Empirical interatomic potential for carbon, with applicaiton to amorphous carbon. *Physical Review Letters* 61, 2879–2882.
- Tersoff, J., 1988b. Empirical interatomic potential for silicon with improved elastic properties. *Physical Review B* 38, 9902–9905.
- Tombler, T. W., Zhou, C., Kong, J., Dai, H., Liu, L., Jayanthi, C. S., Tang, M., Wu, S. Y., 2000. Reversible electromechanical characteristics of carbon nanotubes under local-probe manipulation. *Nature* 405, 769–772.

- Treacy, M. M. J., Ebbesen, T. W., Gibson, J. M., 1996. Exceptionally high Young's modulus observed for individual carbon nanotubes. *Nature* 381, 678–680.
- Truesdell, C., Noll, W., 1965. The non-linear field theories of mechanics. In: Flügge, S. (Ed.), *Handbuch der Physik*, vol. 3/3. Springer-Verlag, Berlin.
- Truesdell, C., Toupin, R. A., 1960. The classical field theories. In: Flügge, S. (Ed.), *Handbuch der Physik*, vol. 3/1. Springer-Verlag, Berlin, p. 226.
- Wagner, H. D., Lourie, O., Feldman, Y., Tenne, R., 1998. Stress-induced fragmentation of multiwall carbon nanotubes in a polymer matrix. *Applied Physics Letters* 72, 188–190.
- Wong, E. W., Sheehan, P. E., Leiber, C., 1997. Nanobeam mechanics: Elasticity, strength, and toughness of nanorods and nanotubes. *Science* 277, 1971–1975.
- Yakobson, B. I., Avouris, P., 2001. Mechanical properties of carbon nanotubes. *Carbon Nanotubes* 80, 287–329.
- Yakobson, B. I., Brabec, C. J., Bernholc, J., 1996. Nanomechanics of carbon tubes: Instabilities beyond linear response. *Physical Review Letters* 76, 2511.
- Yao, N., Lordi, V., 1998. Young's modulus of single walled carbon nanotubes. *Journal of Applied Physics* 84, 1939–1943.
- Yin, M. T., Cohen, M. L., 1983a. Structural theory of graphite and graphitic silicon. *Physical Review B* 29, 6996.
- Yin, M. T., Cohen, M. L., 1983b. Will diamond transform under megabar pressures. *Physical Review Letters* 50, 2006.

- Yu, M. F., Files, B. S., Arepalli, S., Ruoff, R. S., 2000a. Tensile loading of ropes of single wall carbon nanotubes and their mechanical properties. *Physical Review Letters* 84, 5552.
- Yu, M. F., Lourie, O., Dyer, M. J., Moloni, K., Kelly, T. F., Ruoff, R. S., 2000b. Strength and breaking mechanism of multiwalled carbon nanotubes under tensile load. *Science* 287, 637–640.
- Zanzotto, G., 1996. The cauchy - born hypothesis, nonlinear elasticity and mechanical twinning in crystals. *Acta Crystallography A* 52, 839–849.
- Zhang, P., Huang, Y., Geubelle, P. H., Keein, P. A., Hwang, K. C., 2002. The elastic modulus of single wall carbon nanotubes: A continuum analysis incorporating interatomic potentials. *International Journal of Solids and Structures* 39, 3893–3906.
- Zhou, G., Duan, W., Gu, B., 2001. First-principles study on morphology and mechanical properties of single-walled carbon nanotube. *Chemical Physics Letters* 333, 344–349.

VITA

Yongzhe Tian was born in Shenyang (China) on October 18, 1976. He received his Bachelor of Engineering in materials science and engineering from Dalian University of Technology in August 1998 and Master of Science in aerospace engineering from Texas A&M University in August 2005. He can be contacted through his parents at their permanent address: 4-3-2 42-4 baisan lu yuhong qu, Shenyang, China.

The typist for this thesis was Yongzhe Tian.